AD-A046 609 DAVID W TAYLOR NAVAL SHIP RESEARCH AND DEVELOPMENT CE--ETC F/G 13/10
FATIGUE AND CRACK-GROWTH ANALYSES OF HYDROFOIL BOX BEAMS.(U)
OCT 77 N V MARCHICA, L L ICHTER

UNCLASSIFIED DTNSRDC-77-0097 NL

1 OF 2
AD A046609

END
DATE FILMED
12-77
DDC

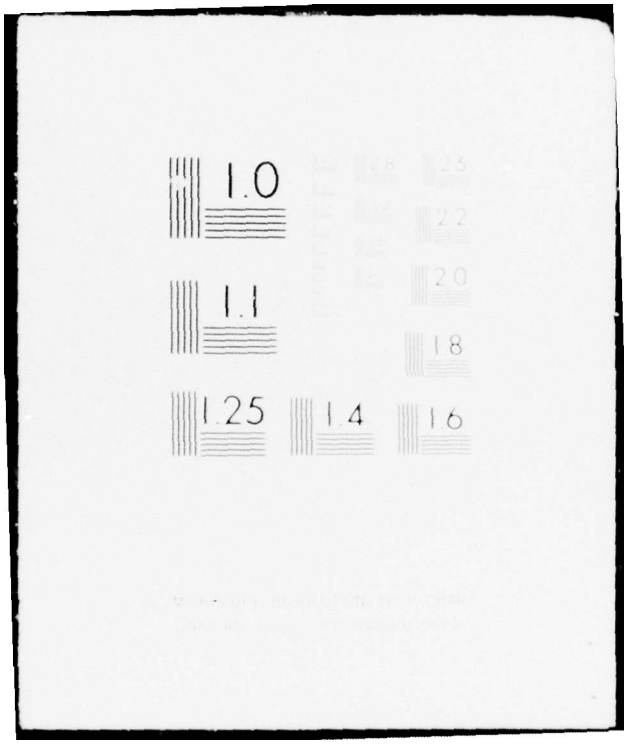
1.0
1.1
1.25
1.4
1.6

Report 77-0097

FATIGUE AND CRACK-GROWTH ANALYSES OF HYDROFOIL BOX BEAMS

12

DAVID W. TAYLOR NAVAL SHIP RESEARCH AND DEVELOPMENT CENTER

Bethesda, Md. 20084

FATIGUE AND CRACK-GROWTH ANALYSES OF HYDROFOIL BOX BEAMS

by

Nicholas V. Marchica and Larry L. Ichter

STRUCTURES DEPARTMENT
RESEARCH AND DEVELOPMENT REPORT

October 1977

Report 77-0097

MAJOR DTNSRDC ORGANIZATIONAL COMPONENTS

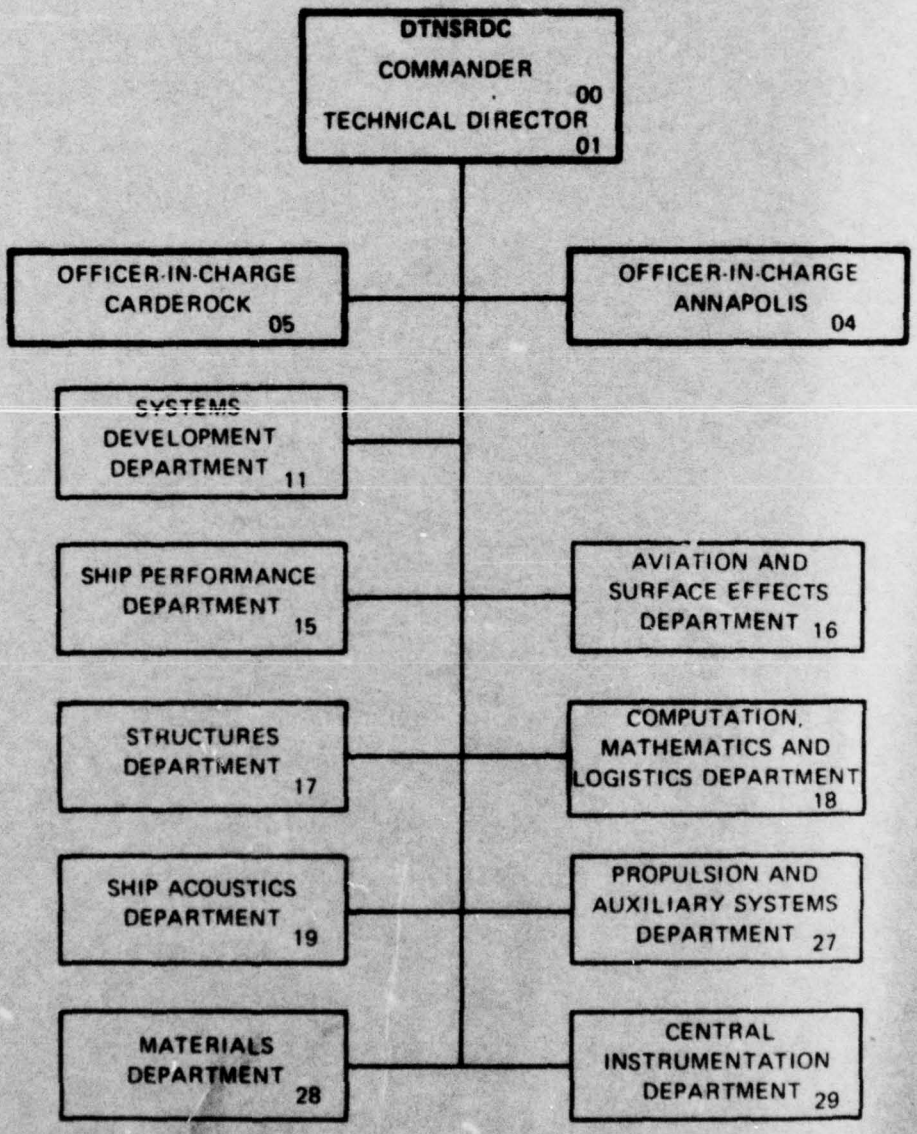

UNCLASSIFIED

SECURITY CLASSIFICATION OF THIS PAGE (When Data Entered)

REPORT DOCUMENTATION PAGE	READ INSTRUCTIONS BEFORE COMPLETING FORM
1. REPORT NUMBER: DTNSRDC-77-0097	2. GOVT ACCESSION NO. / 3. RECIPIENT'S CATALOG NUMBER
4. TITLE (and Subtitle): FATIGUE AND CRACK-GROWTH ANALYSES OF HYDROFOIL BOX BEAMS	5. TYPE OF REPORT & PERIOD COVERED / 6. PERFORMING ORG. REPORT NUMBER
7. AUTHOR(s): Nicholas V. Marchica and Larry L. Ichter	8. CONTRACT OR GRANT NUMBER(s)
9. PERFORMING ORGANIZATION NAME AND ADDRESS: David W. Taylor Naval Ship Research and Development Center, Bethesda, Maryland 20084	10. PROGRAM ELEMENT, PROJECT, TASK AREA & WORK UNIT NUMBERS: (See reverse side)
11. CONTROLLING OFFICE NAME AND ADDRESS	12. REPORT DATE: October 1977 / 13. NUMBER OF PAGES: 96
14. MONITORING AGENCY NAME & ADDRESS(if different from Controlling Office)	15. SECURITY CLASS. (of this report): UNCLASSIFIED / 15a. DECLASSIFICATION/DOWNGRADING SCHEDULE

16. DISTRIBUTION STATEMENT (of this Report)

APPROVED FOR PUBLIC RELEASE: DISTRIBUTION UNLIMITED

17. DISTRIBUTION STATEMENT (of the abstract entered in Block 20, if different from Report)

Research and development rept.,

18. SUPPLEMENTARY NOTES

F43422

SF4342251, SF4342251

19. KEY WORDS (Continue on reverse side if necessary and identify by block number)

Fatigue, Hydrofoil
Crack-Growth
Fracture Mechanics

20. ABSTRACT (Continue on reverse side if necessary and identify by block number)

Fatigue and crack-growth analyses are presented for seven hydrofoil-foil structures (box beams) tested at the David W. Taylor Naval Ship Research and Development Center. The box beams were constructed of materials and details representative of full-scale foil structures. All box beams failed before expiration of their designed duration. Results of the

(Continued on reverse side)

DD FORM 1 JAN 73 1473 EDITION OF 1 NOV 65 IS OBSOLETE
S/N 0102-LF-014-6601

UNCLASSIFIED

SECURITY CLASSIFICATION OF THIS PAGE (When Data Entered)

387 682

(Block 10)

T.A. 43.422.505
T.A. 43.422.506;
W.U.'s 1-1730-312
and 1-1730-342

(Block 20 continued)

analyses indicate these procedures can be used to predict failure in the box beams. Stress-concentration factors and residual stresses were assumed in the fatigue analyses. Initial flaw sizes, based on nondestructive test techniques, were assumed in the crack-growth analyses.

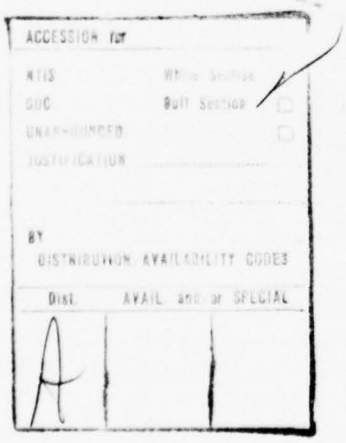

TABLE OF CONTENTS

LIST OF FIGURES

Page

LIST OF TABLES

ABSTRACT

Fatigue and crack-growth analyses are presented for seven hydrofoil-foil structures (box beams) tested at the David W. Taylor Naval Ship Research and Development Center. The box beams were constructed of materials and details representative of full-scale foil structures. All box beams failed before expiration of their designed duration. Results of the analyses indicate these procedures can be used to predict failure in the box beams. Stress-concentration factors and residual stresses were assumed in the fatigue analyses. Initial flaw sizes, based on nondestructive test techniques, were assumed in the crack-growth analyses.

ADMINISTRATIVE INFORMATION

This work was funded and authorized by the Naval Sea Systems Command (03511) under Task Areas 43.422.505 and 43.422.506, Work Units 1-1730-312 and 1-1730-342 for Fiscal Years 1976-77.

INTRODUCTION

A large-scale fatigue evaluation of hydrofoil-foil structures (box beams) is being conducted at the David W. Taylor Naval Ship Research and Development Center. One segment of the hydrofoil, tapered-box beam program[1] is the analysis of fatigue and crack-growth behavior of the structural elements. Fatigue and crack-growth analyses of seven hydrofoil box beams are presented using predictive techniques for cumulative damage and linear elastic fracture mechanics.

BOX-BEAM DESCRIPTION AND TESTING METHOD

The box beams are representative of actual hydrofoil geometry and fabrication details. The forward foil of HIGH POINT (PCH-1) (Figure 1) was used as the basis for the design of the box-beam test section; see Figure 2. The cross directional arrangement of the internal stiffeners is called "egg crate" construction. This type of construction, which is

---

[1]Beach, J.E. et al., "A Large-Scale Fatigue Evaluation of Hydrofoil-Foil Structures," SNAME/AIAA Advanced Marine Vehicles Conference (17-19 Apr 1978. A complete listing of references is given on page 83.

typical of welded hydrofoil foils and struts in general, requires single-sided welds to connect the cover plating to the internal stiffeners (close-out) in the center section. Three methods of closure are shown in Figure 3. The fatigue performance of these single-sided welds is considered poor. Access from one side only limits the capabilities of the welder and the nondestructive testing (NDT) of the weld, thereby increasing the probability of large defects being built into the structure.

The design of the basic hydrofoil-type, box beam is a tapered test section 48-in. in length, having a solid "tongue" added at the top for load application and a 6-in transition to a solid plate added at the bottom to eliminate stress concentrations. The slot-weld configuration of box beams 1, 2, and 4 (1/2-in. HY-80 steel) is shown in Figure 4. The patch configuration of box beam 3 (HY-80) is shown in Figure 5.

HY-130 and 17-4PH stainless steel are two other materials that are being considered for hydrofoil-foil applications. The external geometry of the box beams is not changed. Based on the ratio of the yield strength of the new material to that of HY-80, and considering commonly available plate thicknesses, the plating thickness changes—3/8 in. for HY-130 and 5/16 in. for 17-4PH steels. Box beams 5 and 6 are made of HY-130, while box beams 7 and 8 are constructed of 17-4PH. Box beam 7 has a T-weld configuration (Figure 6) while Table 1 gives the material, configuration, and test environment of each box beam.

Development of the foil-load spectrum is discussed in Reference 1. Figure 7 shows the spectrum as a percentage of yield strength, applied to each box beam. The maximum stress for each box beam is determined from maximum load and measured sensitivity found from static tests, using the following equation

$$\sigma_{Max} = (P_{Max}) \cdot (\text{sensitivity}) \qquad (1)$$

Table 2 presents the maximum stresses for box beams 2 through 8, and Table 3 shows the stress spectra applied to box beams 2 through 8.

FAILURE LOCATIONS

The box beams were designed to last for 7.5×10^6 cycles — 7500 blocks of 1000 cycles per block; however, all box beams tested developed fatigue failures before attaining the designed measure. A fatigue failure was considered to be the first visible through crack occurring in the box-beam test section. Box beam 1 experienced a static overload failure and has not been included in the subsequent analyses. Table 4 gives the first locations of failure for the box beams.

FATIGUE ANALYSES

Fatigue analyses were performed on each box beam, using the Palmgren-Miner cumulative damage theory[2,3] in association with the Goodman law.[4]

Cumulative damage theory assumes failure when

$$\Sigma n_i/N_i = 1.0 \tag{2}$$

where n_i equals the number of cycles at stress level i, and N_i equals the number of cycles at stress level i to cause failure. N_i is determined from fatigue data for basic materials, presented as stress-versus-life (S-N) diagrams. These small specimens are usually tested under fully reversed conditions (R=-1). The stresses applied to the box beam are not fully reversed; however, an equivalent fully reversed stress is found using the Goodman law[4]

$$\sigma_{an} = \sigma_n(1 - \sigma_m/\sigma_u) \tag{3}$$

where σ_{an} = fatigue strength at a given stress ratio

σ_n = fatigue strength at R=-1

σ_m = mean value of alternating stress

σ_u = ultimate material tensile strength

---

[2]Palmgren, A., "Die Lebanstauer Von Kugellagern," VDI-Z, Vol. 68 (1924).

[3]Miner, M.A., "Cumulative Damage in Fatigue," Journal of Applied Mechanics, Vol. 12 (1945).

[4]Richards, C.W., "Chapter 9, Engineering Materials Science," Wadsworth Publishing Company, San Francisco (1961).

σ_n is the unknown equivalent fatigue strength at R=-1

$$\sigma_n = \sigma_{an}\left(\frac{\sigma_u}{\sigma_n - \sigma_m}\right) \tag{4}$$

The equivalent stress spectra for box beams 2 through 8 are shown in Table 5.

Fatigue life calculations were made, using a number of S-N curves for each box beam. The calculations of fatigue life for each box beam are given in Appendix A.

FATIGUE-ANALYSES RESULTS

Table 6 gives the results of the fatigue analyses, comparing them to actual box-beam failures. Notch conditions (K_t=3 to 3.26) were assumed representative of an as-welded condition. This assumption seems valid for some of the box beams.

Two alternative explanations for actual failures occurring sooner than predicted are: (1) either the actual stress-concentration factors K_t in the box beams were greater than 3.0, or (2) the box beam in the as-welded condition contained residual stresses.

An analysis method similar to one used by Boeing in the PHM (patrol combatant missile – hydrofoil) producibility study[5] was used to determine the notch condition that would cause failure in the box beam. A relationship is established between K_t and the fatigue strength at a given number of cycles, e.g., 10^5 or 10^6 cycles, where most of the fatigue damage occurs. As a general rule, a 20-percent decrease (increase) in fatigue strength will halve (double) the fatigue life.* Baseline calculations, using box-beam spectra, supported this. Table 7 presents the notch conditions thus calculated in Appendix A. The range of notches determined are within typical K_t's for as-welded structure as reported by Ellingwood and Lomacky at the Center, except for box beam 4.

---

[5]Bixler, W.D. and D.D. Miller, "Slow Crack Growth, Fracture, Fatigue and Corrosion Assessment of Production PHM Struts and Foils," Boeing Document D312-80437-1 (1975).

*Conversation with Mr. D.D. Miller, Boeing Marine Systems. Boeing Co.

Tensile residual stresses were included in the performed analyses of box-beam spectra and fatigue. These stresses increased the mean-stress levels, thereby increasing the calculated equivalent fully reversed stress range. The residual stresses necessary to cause failure in the box beams, based on representative as-welded conditions — K_t=3.0 to 3.26, are given in Table 8, based on calculations presented in Appendix A. The residual tensile stresses necessary for failure are within reported values.[6] Residual stresses resulting from welding are reduced by postweld, thermal stress relief, heat treatment.[7] Box beam 7 went through an aging cycle at 1100 F, resulting in partial stress relief. Box beam 8 was solution treated at 1900 F then aged at 1100 F, resulting in full stress relief.

CRACK-GROWTH ANALYSES

Crack-growth analyses were used to predict the lives of the box beams subjected to load spectra. These analyses were performed using the theory of linear elastic-fracture mechanics. Both surface flaws and through-the-thickness cracks were modeled, and their growth was calculated.

Crack-growth rate is assumed to be governed by

$$\frac{da}{dN} = \frac{C(\Delta K)^n}{F(K)} \tag{5}$$

where a = either crack depth for surface flaws or half-crack length for through-the-thickness cracks

N = number of cycles of load

C,n = material constants

F(K) = 1 for PARIS equation

= $(1-R)K_c-\Delta K$ for FORMAN equation

ΔK = stress-intensity range at crack tip

R = ratio of minimum to maximum stress for each load cycle

K_c = critical stress-intensity factor for unstable crack growth

---

[6]"Structural Steel Design," Edited by L. Tall, Ronald Press Company, New York (1974).

[7]"Welding Handbook, Section 1," Edited by A.L. Phillips, American Welding Society, p. 5.29 (1969).

The main variable determining crack growth is the stress intensity factor. The equation used to calculate stress-intensity range at the crack tip was

$$\Delta K = 1.1\ \Delta\sigma\sqrt{\frac{\pi a}{Q}}\ M_k \quad \text{for surface flaws} \tag{6a}$$

or

$$\Delta K = \Delta\sigma\sqrt{\pi a}\ \ F(a/w) \quad \text{for through cracks} \tag{6b}$$

where $\Delta\sigma$ = nominal stress range

M_k = backface correction factor

Q = flaw-shape parameter

$$= E^2 - 0.212\left(\frac{\sigma}{\sigma_y}\right)^2$$

where E = elliptical integral of the second kind for the surface flaw. The following term is used to apply a correction for a through crack in a finite-width plate.

$$F(a/w) \doteq \sqrt{\sec\frac{\pi a}{2b}} \tag{7}$$

where b = half-width of plate. The analyses were performed using a modified version of a crack-growth computer program, CRACKS II.[8] The program was modified to allow for varying surface-flaw shapes. This and other modifications are discussed in detail in Reference 9. Analyses were performed for various flaws, using the Paris and Forman equations both with and without retardation. The Willenborg retardation model was used with an assumed plane-stress yield zone. Retardation accounts for residual compressive stresses at the crack tip induced by high-tensile overloads. The crack then takes time to progress through the yield zone, slowing crack growth for the subsequent smaller loads. By using the Willenborg model, reduced effective stresses may be calculated for the lower loads to retard the crack growth.

---

[8] Engle, R.M., "CRACKS II User's Manual," Structures Department, Air Force Flight Dynamics Laboratory, Dayton, Ohio, AFFDL-TM-74-173 (1974).

[9] Marchica, N.V. et al., "A Fatigue Crack Propagation Analysis Program Using Interactive Computer Graphics," Symposium on Applications of Computer Methods in Engineering (23-26 Aug 1977).

The material crack-growth constants are calculated from available da/dN versus ΔK data. These constants vary according to material, environment, stress ratio, and testing technique. For each type of material and environment there is usually a wide scatter of data.[10] Crack-growth constants used in these analyses represent upper-bound (fastest rates) growth data. This assumption would be a conservative estimate used in design. Most crack-growth data are obtained at ΔK levels from 20 to 100 ksi $\sqrt{in}$. A curve is fitted to these data on a log-log plot so that C and n constants of Equation (5) can be determined. This represents the best estimate of crack growth between the ΔK levels. The curve is then extrapolated to lower ΔK levels until the threshold ΔK (ΔK_{th}) is reached. The actual growth relationship would be as shown in Figure 8. This extrapolation can result in error for loads that produce low ΔK levels, typical for surface flaws. These kinds of data are difficult and costly to obtain, so, usually, the original curve must be extrapolated. However, crack-growth data at low ΔK are needed.

Initial flaw size and shape are major assumptions in a crack-growth analysis. These are critical because they determine the stress-intensity range ΔK and, thus, the crack growth. Even slight changes in flaw size and shape can significantly alter the crack growth and the life of the box beams. Initial flaw sizes were based on the smallest crack that could be detected using NDT techniques. Limits for the eddy-current, X-ray, and ultrasonics methods were used for initial flaw sizes; see Figure 9.

Analyses were performed on each box beam to predict the time to first failure. Failure is defined as the time for a surface flaw to grow to a through-the-thickness crack. Predictions were made, using the three initial flaw shapes and the Paris and Forman equations with and without the effects of retardation. Twelve different life predictions were made for each box beam; results of these analyses are given in Appendix B.

---

[10] Clark, W.G. and S.J. Hudak, Jr., "Variability in Fatigue Crack Growth Rate Testing," Journal of Testing and Evaluation, Vol. 3 (Nov 1975).

After a through crack appears in the box beam, additional load applications will result in further crack growth. Crack-length measurements can be taken during the testing, providing specific data for crack length versus number of load blocks. Analyses can then be performed by knowing the initial crack length that was measured. Predictions can be made using Paris and Forman equations with and without retardation. Some of the crack-growth measurements were taken for a limited crack length or number of load blocks, and no predictions of growth were made. Box beams 5 through 7 contained through cracks that provided enough data to compare with predictions. Since initial and intermediate crack lengths were known, conclusions could be made as to which model produced the best results. Also different crack-growth data could be used to calculate C and n, which might give closer predictions. Data and results of through-crack growth are presented in Appendix C.

CRACK-GROWTH ANALYSES RESULTS

SURFACE FLAWS

Surface-flaw analyses were used to try to predict the time to first failure of each box beam. Detailed results are given in Appendix B. Table 9 contains the closest predictions for each box beam. Two possible situations could exist to explain discrepancies in actual versus predicted lives. They are either (1) an initial flaw size that was different from that assumed, or (2) crack-growth data, used to calculate the constants C and n for Equation (5), did not adequately represent crack growth in the box beam. As the crack-growth data used were upper-bound (faster growth) data, a shorter life prediction would most likely occur.

The ultrasonic surface flaw, combined with the Forman-unretarded equation, came closest to predicting failure for HY-80 box beams 2 through 4. All other predictions were much greater than the actual life.

The Paris equation came closest to predicting failure for the eddy-current flaw in HY-130 box beams 5 and 6. Retardation gave the closest values for box beam 5 in saltwater, while the unretarded equation gave a better fit for box beam 6 in air.

The duration of box beam 7, tested in saltwater, was best predicted for an X-ray flaw with a Forman retarded equation. This box beam was constructed of vacuum-melted 17-4PH, directly aged at 1100 F, having a yield stress of 112 ksi.

Box beam 8 was constructed of vacuum-melted solution-treated and aged 17-4PH H 1100 and was tested in saltwater. This material had a yield stress of 153 ksi. The Paris-retarded equation with eddy-current and X-ray flaws gave the closest values of predicted life.

THROUGH CRACKS

Crack-growth data were available for three through cracks each on box beams 5 and 6 and for one through crack each on box beams 7 and 8. Due to limited data for some of the cracks, only four cracks were used to check predicted values. Since specific crack-growth data are available, these analyses should give the best indication as to which model — equation and retardation — is most applicable for each box beam. The complete analyses are contained in Appendix C.

For all the box beams, the Paris "retarded" model fits the data best. Over the whole time of growth this model "predicted" slightly faster growth than actually occurred, except for box beam 7, where it showed slightly slower growth. To make comparisons, material constants C and n were calculated for lower-bound (slower) crack-growth data and for the average of lower- and upper-bound data. These constants were used to make new predictions using the Paris retarded model on box beams 5 and 6 and with the Paris "unretarded" model on box beam 7. Results are shown in Figures 10 through 13. The average values came closest to predicting the crack growth for each of the through cracks.

FURTHER ANALYSIS OF SURFACE FLAWS

Using the models which best predicted the through-crack growth, analyses were performed again for various initial flaws in box beams 5 through 7; see Appendix D. For box beam 5, having average material constants, the X-ray-flaw analysis predicted failure within 8 percent of the actual life. No other significantly better predictions were shown.

NOTCH ANALYSES

A notch-deformation and cumulative damage-analysis computer program DEFRESP* was used to determine the crack-initiation periods for box beams 2 through 8. The stress-strain history at the notches was simulated, based on properties of basic materials, stress level, and notch geometry. A range of fatigue strength-reduction factors K_f was assumed for the analyses. The damage accumulation algorithm is

$$D_i = \frac{1}{N_i} = \left(\frac{\Delta\varepsilon_{Ti}}{c}\right)^{1/m} \tag{8}$$

where m and c are experimental regression constants

$\Delta\varepsilon_{Ti}$ is the i^{th} strain-amplitude reversal

N_i is the i^{th} equivalent fully reversed cycle.

Initiation occurs when the accumulated damage reaches unity. Results of the analyses are presented in Appendix E.

Stress concentration factors K_t were determined for the assumed initial flaws used in the crack-growth analyses. Table 10 gives the notch geometries for the eddy-current, ultrasonic, and X-ray flaws. The K_t for each condition was determined, using the following equations from Reference 6

$$K_t = 1 + 2\sqrt{a/\rho} \tag{9}$$

$$K_t = (0.78 + 2.24\sqrt{a/\rho} \tag{10}$$

*Developed by B. Ellingwood and D. Martin at the Center in June 1976.

for $1 < a/\rho < 360$

$$K_t = 1 + (K_f - 1)/q \qquad (11)$$

where $q = \dfrac{1}{1 + \left(\dfrac{0.0137}{\rho}\right)^{0.76}}$ for $\rho \leq 0.10$

A comparison of these three equations, where applicable, using the three surface-flaw geometries is given in Table 11. Using K_f=2.5 in Equation (11) for the ultrasonic and eddy-current flaws gives similar K_t's as calculated by Equations (9) and (10). The K_f for the eddy-current flaw could not be determined from Equation (11). The fatigue-strength, reduction factor can be conservatively estimated by assuming $K_f = K_t$.[6] A K_f of 2.0 was selected for the eddy-current flaw.

Total predicted life is determined by adding the predicted flaw-growth life and the predicted initiation life; see Table 12. The initiation period is a small percentage of the total predicted life (5.1-percent average) and the actual test life (5.4-percent average); see Table 13.

CONCLUSIONS

1. All box beams tested failed before expiration of their design life of 7500 spectra = 7.5×10^6 cycles.

2. Fatigue analyses showed that stress-concentration factors from 2.4 to 7.7 and/or residual stresses from 6 to 33 ksi were necessary to predict failure in each of the box beams.

3. Crack-growth analyses, using linear elastic fracture mechanics, showed that initial flaws, based on NDT methods, can be used in predicting failure in the box beams.

4. Through-crack growth can be accurately predicted, using the Paris equation with the Willenborg retardation model for the HY-130 box beams and the Paris equation without retardation for the 17-4PH, directly aged box beam.

5. The crack-initiation period, determined by notch-deformation analyses, is a small percentage (5.1-percent average) of the total predicted life of each box beam.

ACKNOWLEDGMENTS

The authors would like to thank Mr. Steve Zemanek for recording crack-growth measurements, Mr. Don Martin for performing the notch analyses, and Mr. Jeff Beach, project manager, and Mr. Nat Nappi for providing constructive comment in the review of the report.

APPENDIX A

FATIGUE ANALYSES

Calculations for the fatigue analyses of box beams 2 through 8, based on the Palmgren-Miner cumulative damage theory, are presented in this appendix.

1. BOX BEAMS 2, 3, and 4 — HY-80 STEEL

Thickness = 0.5 inch; Ultimate strength = 103 ksi.

n	σ_{Max} (ksi)	σ_{Min} (ksi)	σ_{Mean} (ksi)	σ_{Alt} (ksi)
1	23.18	0.00	-----	----
544	27.82	18.54	23.18	4.64
1	23.18	-23.18	-----	----
312	33.30	22.20	27.75	5.55
3	52.59	27.75	-----	----
138	38.79	25.85	32.32	6.47

σ_n (ksi)	S_r (ksi)	n/Block
5.99	11.98	544
7.60	15.20	312
9.43	18.86	138
23.18	46.36	1
20.36	40.72	3
14.70	29.57	1

Cumulative damage calculations for box beams 2 and 3 are given in Table 14 based on S-N curves of Figure 14. Results indicate an assumed notch condition K_t=3.26 will cause failure in 8031 spectra. Actual failures for box beams 2 and 3 were 7080 and 4170 spectra, respectively.

A relationship is established between stress concentration and fatigue strength at 10^6 cycles, fatigue quality rating, for HY-80* and HY-100[11] tested in seawater; see Figure 15. A 20-percent decrease (increase) in

*U.S. Naval Engineering Experiment Station, Computer Printout EES 910 178 420/66.

[11]Gross, M.R. and E.J. Czyryca, "Effects of Notches and Salt Water Corrosion on the Flexural Fatigue Properties of Steels for Hydrospace Vehicles," Naval Engineers Journal (Dec 1967).

fatigue strength will halve (double) the fatigue life.* The notch condition thus calculated for box beam 2 is 3.7; for box beam 3, k_t=6.7.

Residual stresses of 10, 15, 20, and 30 ksi were assumed for box beams 2 and 3, and fatigue lives were determined. The results are presented in Figure 16. The residual stresses determined for K_t=3.25 are 10 ksi for box beam 2 and 20 ksi for box beam 3.

Cumulative damage calculations for box beam 4 are given in Table 15, based on S-N curves of Figure 17. Failure is predicted after 219,600 spectra for K_t=3.26. Box beam 4 failed after 6260 spectra.

A relationship is established between K_t and fatigue strength at 10^6 cycles for HY-80 tested in air in Figure 18.[11,12] The notched condition necessary for the box beam to fail is greater than 20, which is unrealistic.

Residual stresses of 10, 20, 30, and 35 ksi have been assumed in the box beam, and the results are presented in Figure 19. An assumed residual stress of 33 ksi with K_t=3.25 will predict failure in box beam 4.

2. BOX BEAM 5 – HY-130 STEEL

Thickness = 0.375 inch; Ultimate strength = 145.2 ksi.

n	σ_{Max} (ksi)	σ_{Min} (ksi)	σ_{Mean} (ksi)	σ_{Alt} (ksi)
1	36.48	0.00	-----	-----
544	43.78	29.18	36.48	7.30
1	36.48	-36.48	-----	-----
312	52.41	34.93	43.67	8.74
3	82.915	43.67	-----	-----
138	61.04	40.68	50.86	10.18

*Per conversation with Mr. D.D. Miller, Boeing Marine Systems, Boeing Co.

[12]Gross, M.R. and H.C. Ellinghausen, "Investigation of the Fatigue Properties of Submarine Hull Steels, U.S. Naval Engineering Experiment Station, R&D Report 910 178, S-R007-01-01 (31 Aug 1960).

σ_n (ksi)	S_r (ksi)	n/Block
9.75	19.50	544
12.50	25.00	312
15.67	31.34	138
36.48	72.96	1
34.78	69.56	3
23.65	47.31	1

Cumulative damage calculations, based on Boeing S-N data K_t=3.13 of Figure 20,* [13,14] are presented in Table 16. Failure was predicted in 472 spectra compared to 996 spectra to actual failure.

Fatigue strength at 10^6 cycles is related to stress-concentration factor for HY-130 cycled in saltwater in Figure 21. A stress concentration of 2.4 was determined for box beam 5.

3. BOX BEAM 6 — HY-130 STEEL

Thickness = 0.375 inch; Ultimate strength = 152.3 ksi.

n	σ_{Max} (ksi)	σ_{Min} (ksi)	σ_{Mean} (ksi)	σ_{Alt} (ksi)
1	33.88	0.00	-----	-----
544	40.66	27.10	33.88	6.78
1	33.88	-33.88	-----	-----
312	48.67	32.45	40.56	8.11
3	77.01	40.56	-----	-----
138	56.69	37.79	47.24	9.45

*U.S. Marine Engineering Laboratory, Computer Printout MEL365/65 420/66.

[13]Hydronautics, Incorporated, "R.R. Moore Fatigue Data for HY-130 Steel, Test Frequency = 100,000 CPM," (1965).

[14]Miller, D.D., "Hydrofoil Material Evaluation - Base Metal (& Coated Metal) Fatigue and Fracture Studies," Boeing Document D180-15197-3 (Nov 1974).

σ_n (ksi)	S_r (ksi)	n/Block
8.72	17.44	544
11.05	22.10	312
13.70	27.40	138
33.88	67.76	1
29.69	59.38	3
21.58	43.16	1

Cumulative damage calculations, based on Boeing S-N data K_t=3.13 of Figure 22 are presented in Table 17. Failure was predicted in 59,873 spectra, while the actual failure occurred after 2146 spectra.

Fatigue strength at 10^5 cycles is related to the stress-concentration factor for HY-130 cycled in air in Figure 23. A stress-concentration factor of 7.7 was determined for box beam 6.

Residual stresses of 10, 20, 25, and 30 ksi were assumed in the box beam, and results have been shown in Figure 24. An assumed residual stress of 30 ksi with a K_t=3.13 will predict failure in box beam 6.

4. BOX BEAM 7 — 17-4PH DA 1100 STAINLESS STEEL

Thickness = 0.3125 inch; Ultimate strength = 126 ksi.

n	σ_{Max} (ksi)	σ_{Min} (ksi)	σ_{Mean} (ksi)	σ_{Alt} (ksi)
1	26.79	0.00	-----	-----
544	32.15	21.43	26.79	5.36
1	26.79	-26.79	-----	-----
312	38.50	25.66	32.08	6.42
3	60.90	30.08	-----	-----
138	44.84	29.88	37.36	7.48

σ_n (ksi)	S_r (ksi)	n/Block
6.81	13.62	544
8.61	17.22	312
10.63	21.26	138
26.79	53.58	1
22.84	45.68	3
16.95	33.90	1

Cumulative damage calculations were based on the Boeing Company compilation of all available 17-4PH stainless steel data.[5] Figure 25 presents the relationship between stress-concentration factor and fatigue strength at 10^5 cycles as developed in Reference 5. Stress concentrations of 2, 3, and 4 were assumed for box beam 7, and calculations were performed based on Figures 26 through 28, respectively. The results are presented in Table 18. A K_t=3.4 would cause failure (3051 spectra) in box beam 7.

Residual stresses of 5 and 10 ksi were assumed for K_t=3 for box beam 7, and the calculated lives were 3383 and 2196 spectra, respectively. An assumed residual stress of 6 ksi will predict failure in box beam 7.

5. BOX BEAM 8 — 17-4PH H 1100 STAINLESS STEEL

Thickness = 0.3125 inch; Ultimate strength = 158 ksi.

n	σ_{Max} (ksi)	σ_{Min} (ksi)	σ_{Mean} (ksi)	σ_{Alt} (ksi)
1	35.75	0.00	-----	-----
544	42.90	28.60	35.75	7.15
1	35.75	-35.75	-----	-----
312	51.35	34.23	42.79	8.56
3	81.25	42.79	-----	-----
138	59.81	39.87	49.84	9.97

σ_n (ksi)	S_r (ksi)	n/Block
9.24	18.48	544
11.74	23.48	312
14.56	29.12	138
35.75	71.50	1
31.66	63.32	3
22.82	45.64	1

Stress concentrations of 2 and 3 were assumed for box beam 8, and calculations were performed based on Figures 26 and 27, respectively. The results, presented in Table 19, indicate K_t=3.0 will predict failure in box beam 8 (1226 spectra).

APPENDIX B

SURFACE-FLAW ANALYSES

Surface-flaw analyses were performed for each box beam using various initial flaw sizes and model equations. Initial flaws were based on the minimum detectable crack for the following nondestructive testing techniques.

1. Eddy Current
2. Ultrasonics
3. X-Ray

Each flaw was analyzed with Paris and Forman equations, both retarded and unretarded. The process produced 12 predictions for time-to-failure (transition to through crack) for each box beam. Table 20 shows results in terms of number of load blocks to failure. In Table 21 the initial flaws and models used for each analysis and box beam are ranked for closeness of prediction to first failure. Analyses performed using the Forman equation give a much shorter life. This is caused by the majority of the loads in the spectrum having a high-stress ratio R. In the Forman equation for crack growth, higher R-value loads produce higher crack-growth rates for the same stress-intensity range. The Paris equation is based only on stress-intensity range and does not depend on the R.

Crack-growth data used were upper-bound (faster) growth data. A curve fit was used to calculate the constants used in the crack-growth equation. The HY-80 and HY-130, crack-growth rates are shown in Figures 29 and 30. Crack-growth data for HY-80 and HY-130 in air[15] and HY-130 data in saltwater[16] were obtained from U.S. Steel. Very few data are available for HY-80 in saltwater. An assumed rate was calculated by scaling-up the HY-80 air data by the same ratio as the HY-130 crack-growth rate increased

---

[15] Barsom, J.M. et al., "Fatigue-Crack Propagation in High Yield-Strength Steels," Engineering Fracture Mechanics, Vol 2, pp. 301-317 (1971).

[16] Barsom, J.M. et al., "Corrosion-Fatigure Crack Propagation Below K_{ISCC} in Four High-Yield-Strength Steels," United States Steel, Project 89.021-024(3) (14 Dec 1970).

from air to saltwater. Figure 31 shows crack-growth rates for 17-4PH. Argon-oxygen melt, H 1050 data from NRL[17] (Naval Research Laboratory) were used for box beam 7. Vacuum melt H 1050 data, also from NRL,[18] were used for box beam 8.

In HY-80 box beams 2 through 4, the ultrasonic surface flaw with the Forman unretarded equation produced the closest prediction. Other combinations gave lives that were much greater than the actual life. This could be due to the presence of a larger initial flaw size than that assumed or to the crack-growth rates being greater than those represented by data. Since the crack-growth data used to calculate the material constants were upper-bound (faster-growth) data, the assumed initial flaw size was most likely in error.

The eddy-current flaw and the Paris equation analysis best predicted the lives of HY-130 box beams 5 and 6. Equations using the retardation factor produced the closest prediction for box beam 5 in saltwater, while equations using the unretarded parameter gave a better fit for box beam 6 cycled in air. Table 21 shows that the eddy-current flaw with the Paris equation is best for predicting the life of box beam 5. In box beam 6 (air), Paris unretarded and Forman retarded equations in combination with either an eddy-current or an X-ray flaw produce close results.

Box beam 7 was constructed of vacuum melt, 17-4PH, directly aged steel. Since practically no crack-growth data exist for this heat treatment of 17-4PH, argon-oxygen melt H 1050 was used to represent this box beam. Both materials have a fairly low fracture toughness, compared with other heat treatments. Using these crack-growth data to derive material constants, a Forman retarded model works well with either an X-ray or an eddy-current flaw to predict life.

---

[17] Crooker, T.W., "Effect of Heat Treatment on Corrosion-Fatigue Crack Growth," Enclosure to NRL letter 6384-9N (1974).

[18] Crooker, T.W. et al., "Influence of Experimental Factors on Corrosion-Fatigue Crack-Growth Rate Characterization in 17-4PH Steel," Report of NRL Progress, pp. 21-23 (May 1976).

Vacuum-melt, solution-treated and aged, 17-4PH H 1100 steel was used to construct box beam 8, which was cycled in saltwater. The Paris retarded equation model, using either an eddy-current or an X-ray flaw gave the best life-duration predictions.

APPENDIX C

THROUGH-CRACK ANALYSES

Once a through crack appeared in a box beam, measurements could be taken of the growth of this crack. Box beams 5 and 6 had three through cracks each for which data were available; box beams 7 and 8 had one crack each. Some of the measurements were taken in a limited time frame so they did not represent an appreciable amount of growth. Complete data covering a large number of cycles were available for four cracks. These cracks were analyzed using Forman and Paris equations, with and without retardation. Figures 32 through 35 compare predictions for each crack with actual data.

For all box beams, the Paris retarded model fits the actual crack-growth data the best. The Forman retarded and Paris unretarded models give essentially the same results; however, both predict faster growth than actually occurred. The Forman unretarded model does not appear to apply at all to these box beams (5 through 7) as it gives much faster growth than occurs. In reviewing the total growth range, the Paris retarded model seems to give slightly faster growth than occurs, except for box beam 7, which shows slightly slower growth. Since the material crack-growth constants were calculated from data representing the fastest rates of growth, the predicted growth should be an upper bound. This would indicate that the Paris unretarded model better predicts crack growth in box beam 7. For comparison, material crack-growth constants were calculated from lower-bound (slower) growth data and the average of lower and upper bound data. These constants were then used to make new predictions for through cracks with the Paris retarded model for box beams 5 and 6 and the Paris unretarded model as box beam 7. The results of these analyses have been shown in Figures 10 through 13. Crack growth for a majority of the data points is bracketed with the lower- and upper-bound data. The average values come closest in predicting the actual crack growth for each of the four through cracks.

Crack-growth data used for lower-bound rates were obtained from NRL.[17,19,20] Figure 36 shows HY-130 in air; Figures 37 and 38 show HY-130 and 17-4PH, respectively, in saltwater.

---

[19]Crooker, T.W. et al., "Effects of Loading Parameters on Fatigue-Crack Growth in HY-130 Steel," NRL Memorandum Report 2822 (Jun 1974).

[20]Crooker, T.W. and W.R. Cares, "An Exploratory Investigation of Corrosion-Fatigue Crack Growth in HY-130 Base Plate," NRL Memorandum Report 2660 (Oct 1973).

APPENDIX D

SURFACE-FLAW ANALYSES, USING REFINED MODELS

Once the most applicable model is determined from the through-crack analysis (Appendix C) new predictions can be made for the surface-flaw analyses. The initial flaw sizes used are the same as before. The Paris retarded model was used for HY-130 box beams 5 and 6, and the Paris unretarded model was used for box beam 7. The lower-bound and average crack-growth constants were utilized in the new analysis. Results are shown in Table 22.

All three initial flaws were reanalyzed for box beam 5. Predictions of life with the X-ray flaws improved as they did with the ultrasonic flaw. The eddy-current flaw — which had predicted life the best, using upper-bound crack-growth data — showed an increase away from the actual life; however, the prediction was still close to the actual life. Using the average data with the X-ray flaw predicted failure within 8 percent of the actual life for box beam 5.

In box beam 6, HY-130 in air, results predicted by the Paris retarded model for the eddy-current and X-ray flaws were much higher than for the actual life, so these initial flaw conditions were not rerun. The new predicted life, using the ultrasonic flaw equation was closer to the actual life but still less than 50 percent of the life. This would indicate that the initial flaw was larger than either an eddy-current or an X-ray flaw but smaller than an ultrasonic flaw.

In box beam 7 (17-4PH), the lives predicted for eddy-current and X-ray flaws were greater than the actual life, so only an ultrasonic flaw was reanalyzed. This new prediction was much closer than the previous value; however, it was still only 50 percent of the actual life. Again this would show that the initial flaw size was between that of an ultasonic flaw and an X-ray or eddy-current flaw.

APPENDIX E

NOTCH-ANALYSES RESULTS FOR BOX BEAMS 2 THROUGH 8

BOX BEAMS 2, 3 — HY-80, CYCLED IN SALTWATER

Assumed K_f:	Spectra to Initiation
2	414
2.5	206
3	119
4	62
5	35
6	20

BOX BEAM 4 — HY-80, CYCLED IN AIR

Assumed K_f:	Spectra to Initiation
2	461
2.5	245
3	158
4	97
5	60
6	39

BOX BEAM 5 — HY-130, CYCLED IN SALTWATER

Assumed K_f:	Spectra to Initiation
2	199
2.5	72
3	30
4	8
5	3

BOX BEAM 6 — HY-130 CYCLED IN AIR

Assumed K_f:	Spectra to Initiation
2	369
2.5	168
3	86
4	31
5	13
6	7

BOX BEAM 7 — 17-4 PH H 1100 DIRECT-AGE-CYCLED IN SALTWATER

Assumed K_f:	Spectra to Initiation
2	766
2.5	154
3	33
4	3
5	1

BOX BEAM 8 — 17-4 PH H 1100 SOLUTION, TREATED AND AGED, CYCLED IN SALTWATER

Assumed K_f:	Spectra to Initiation
2	77
2.5	14
3	3
4	1

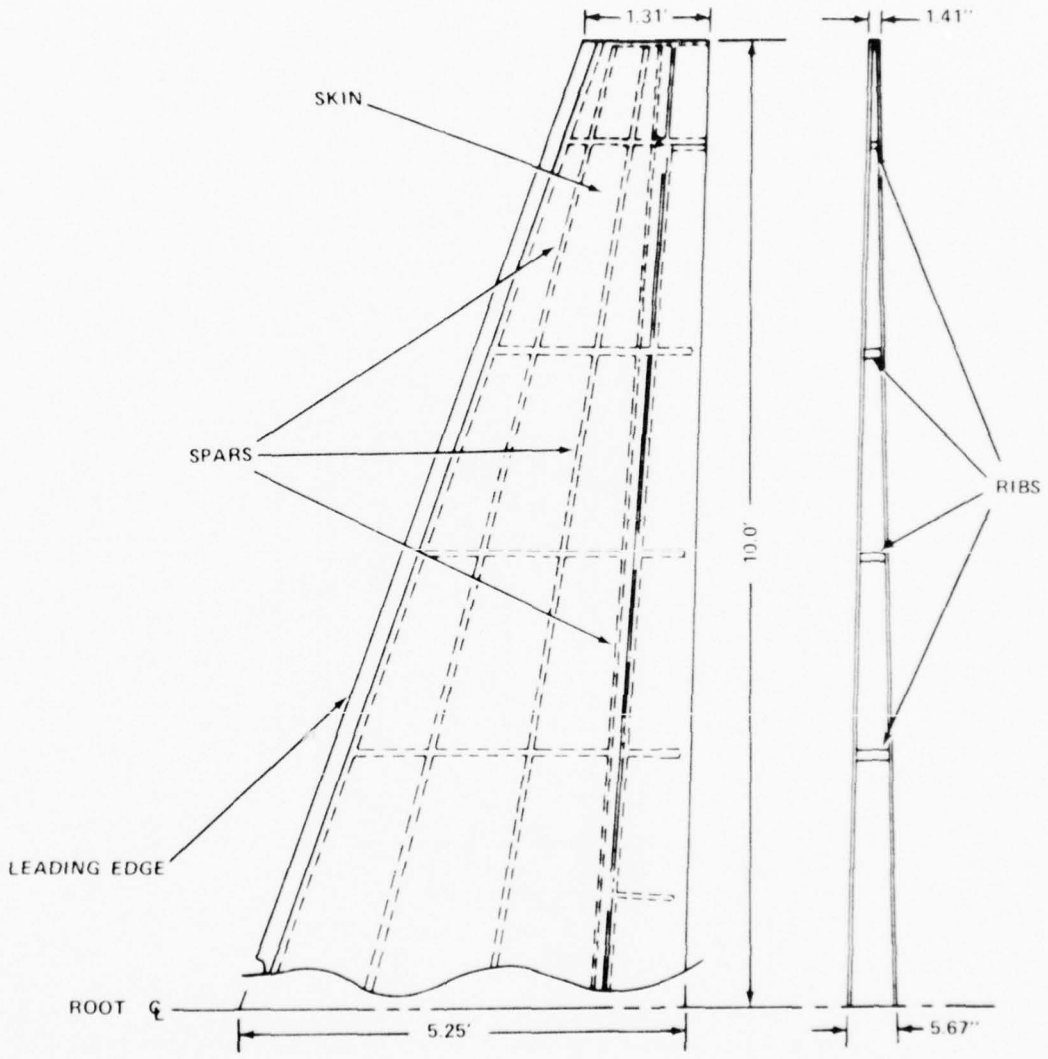

Figure 1 - HIGH POINT (PCH-1) Forward Foil Semispan

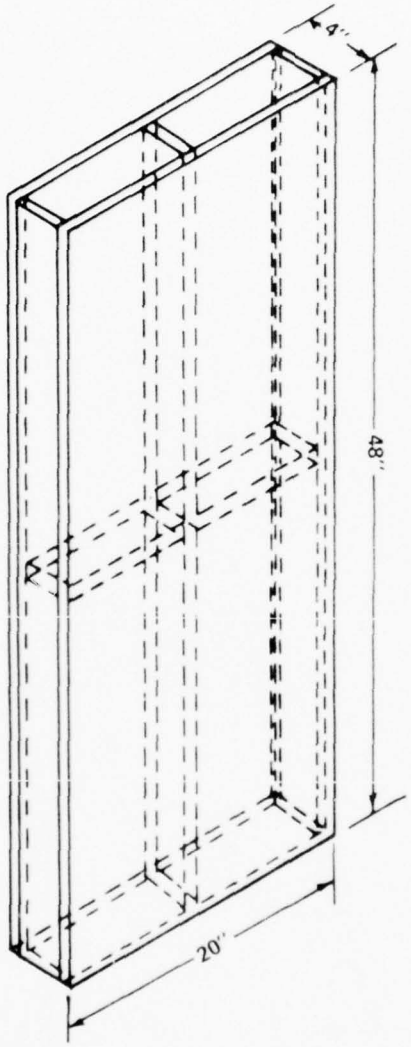

Figure 2 — Basic Box Section with Internal Stiffeners

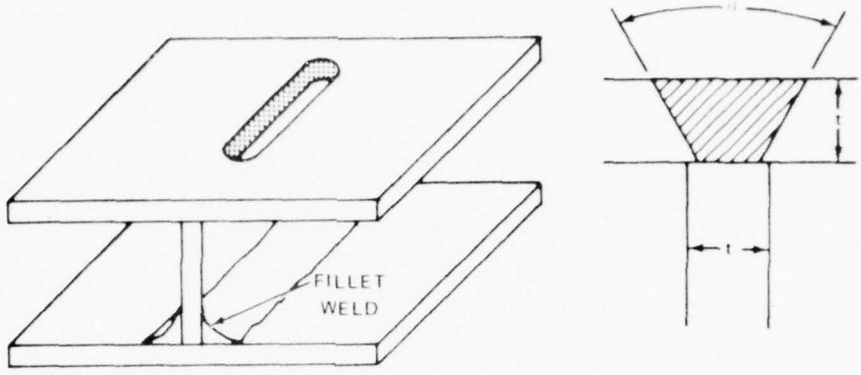

Figure 3a – Slot Weld

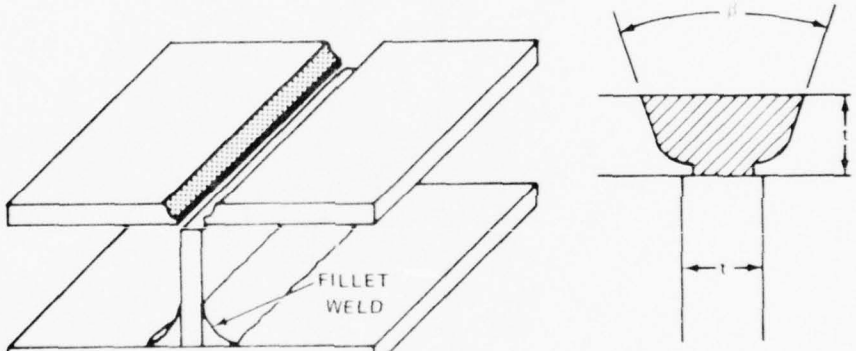

Figure 3b – Single-Sided T–Weld

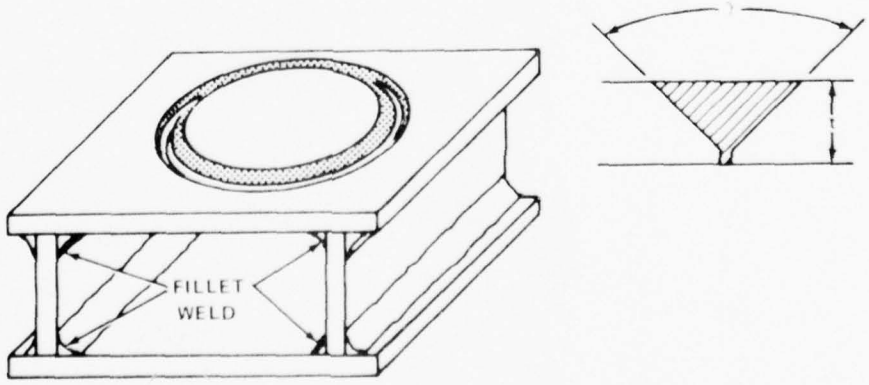

Figure 3c – Single-Sided Butt Weld

Figure 3 – Three Methods of Closure for Foil Structures

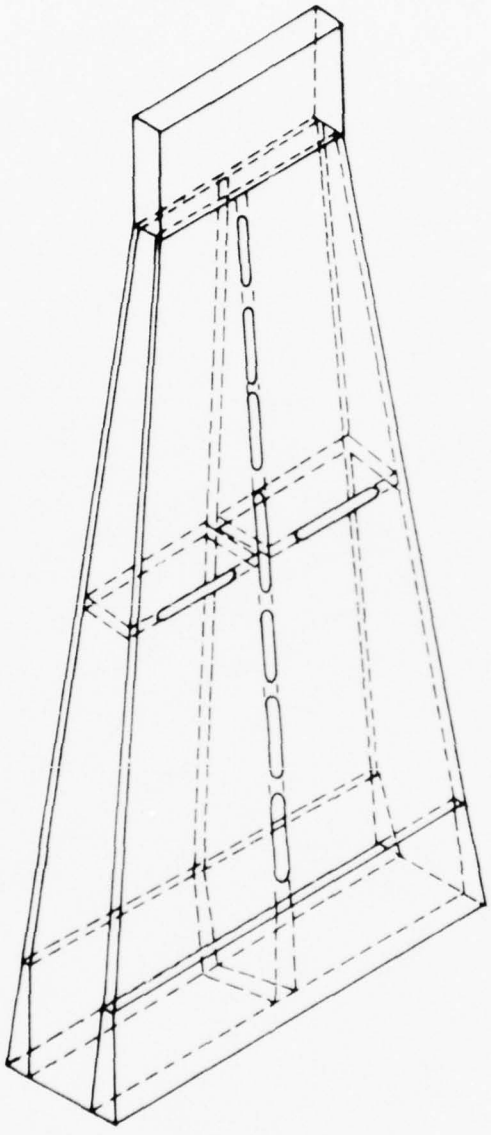

Figure 4 — Basic HY-80 Hydrofoil, Tapered Box Beam;
Slot-Weld Configuration

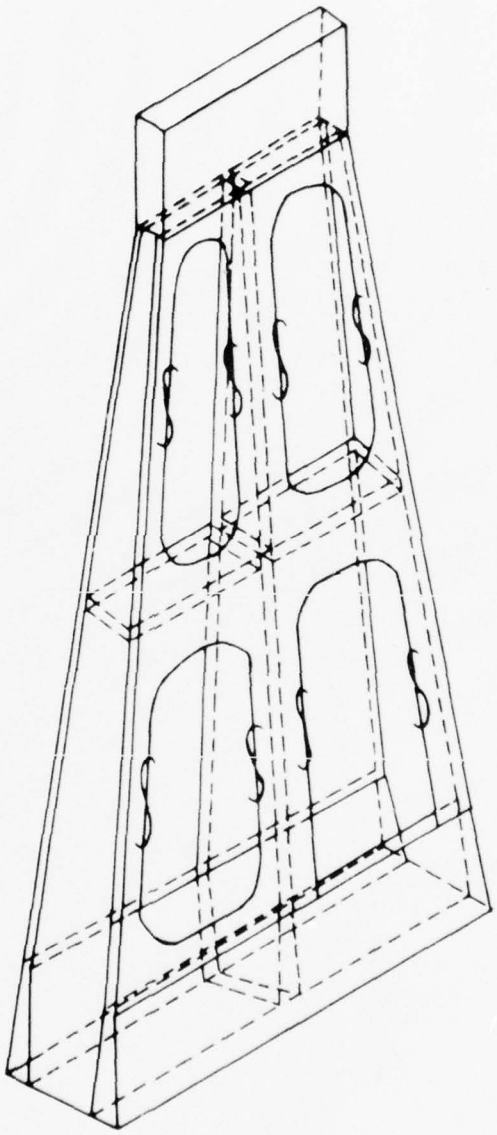

Figure 5 — Box-Beam Design with Closure Patches; Single-Sided Butt Weld

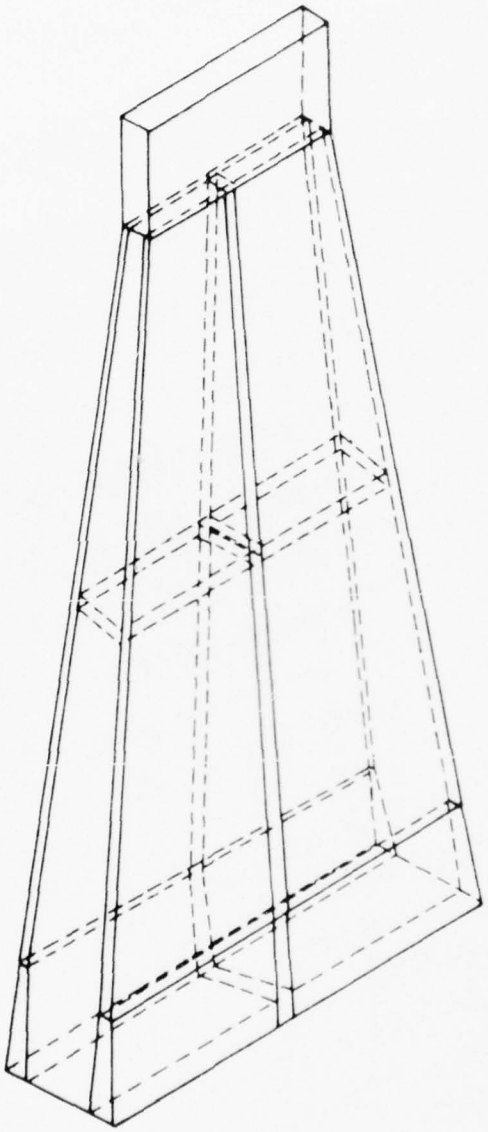

Figure 6 — Box-Beam Design with Continuous Single-Sided T-Welds

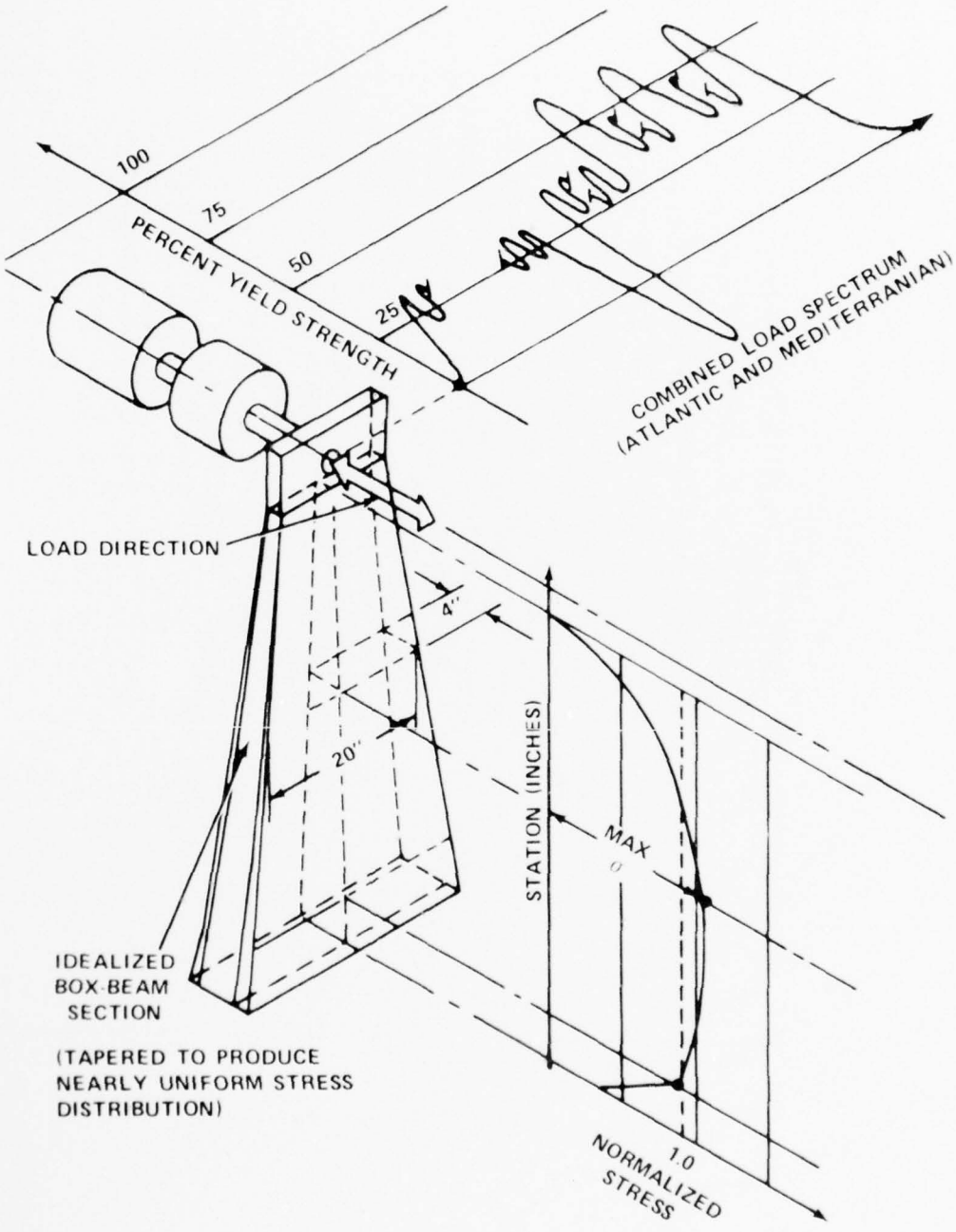

Figure 7 — Hydrofoil Fatigue Element

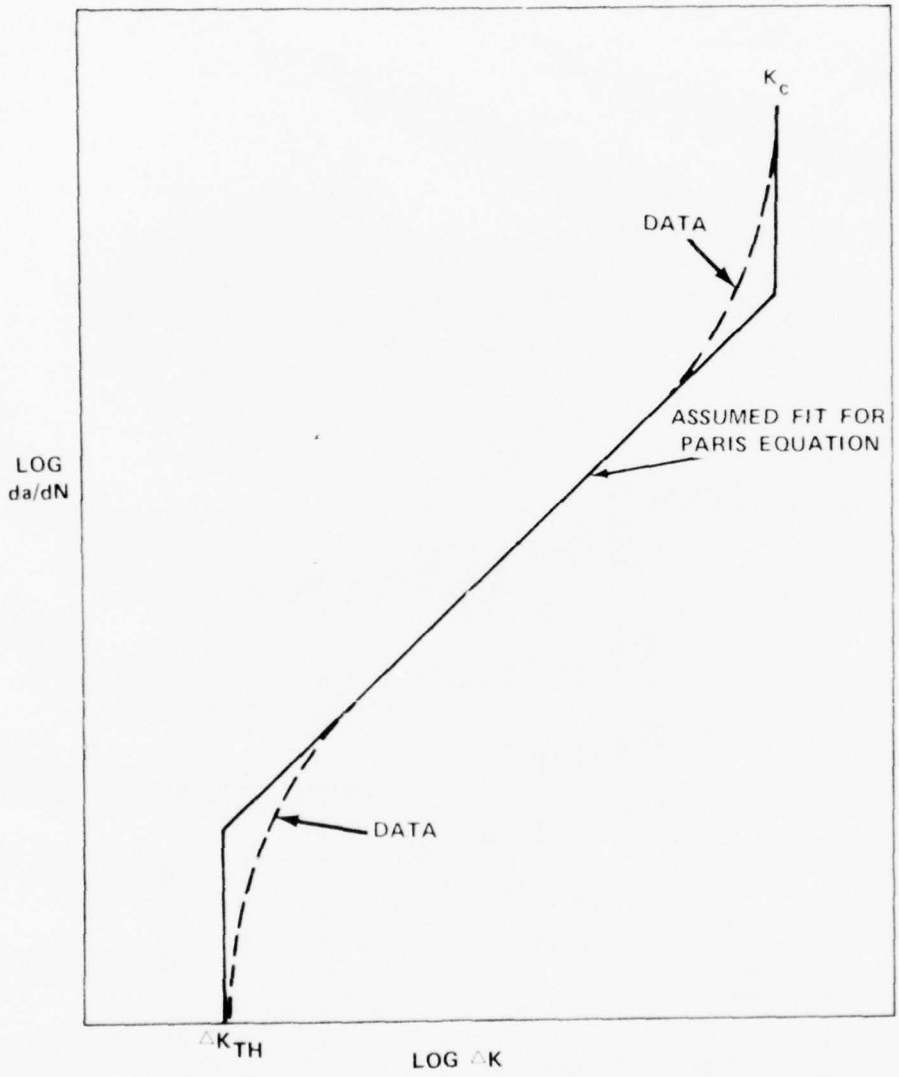

Figure 8 — Crack-Growth Relationship

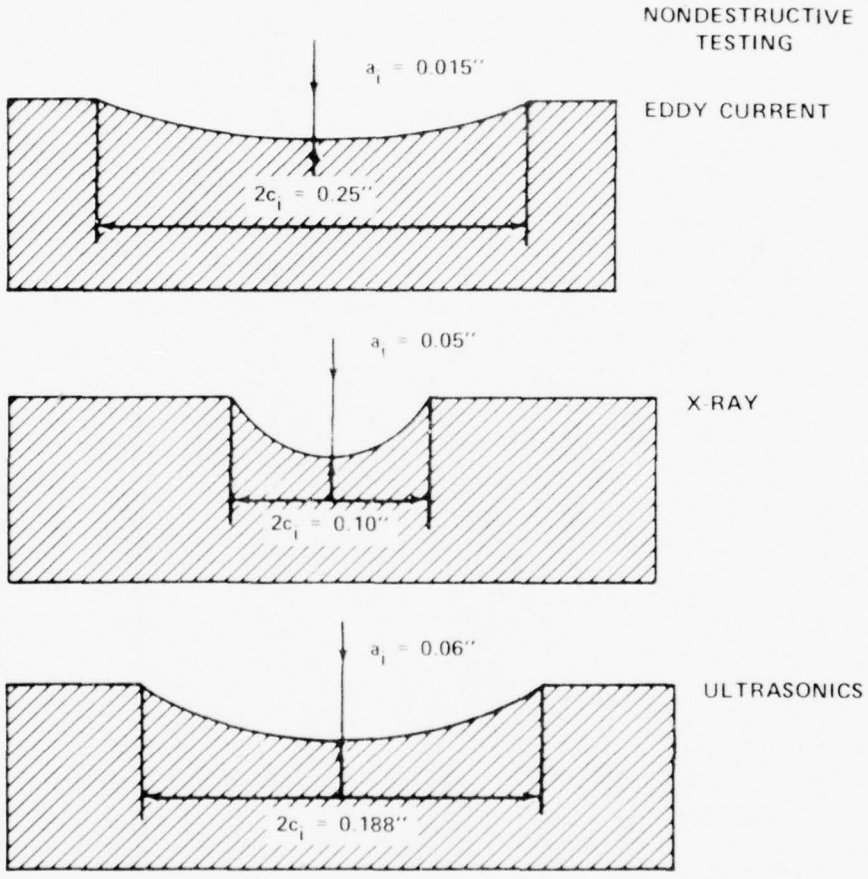

Figure 9 — Assumed Initial Flaws

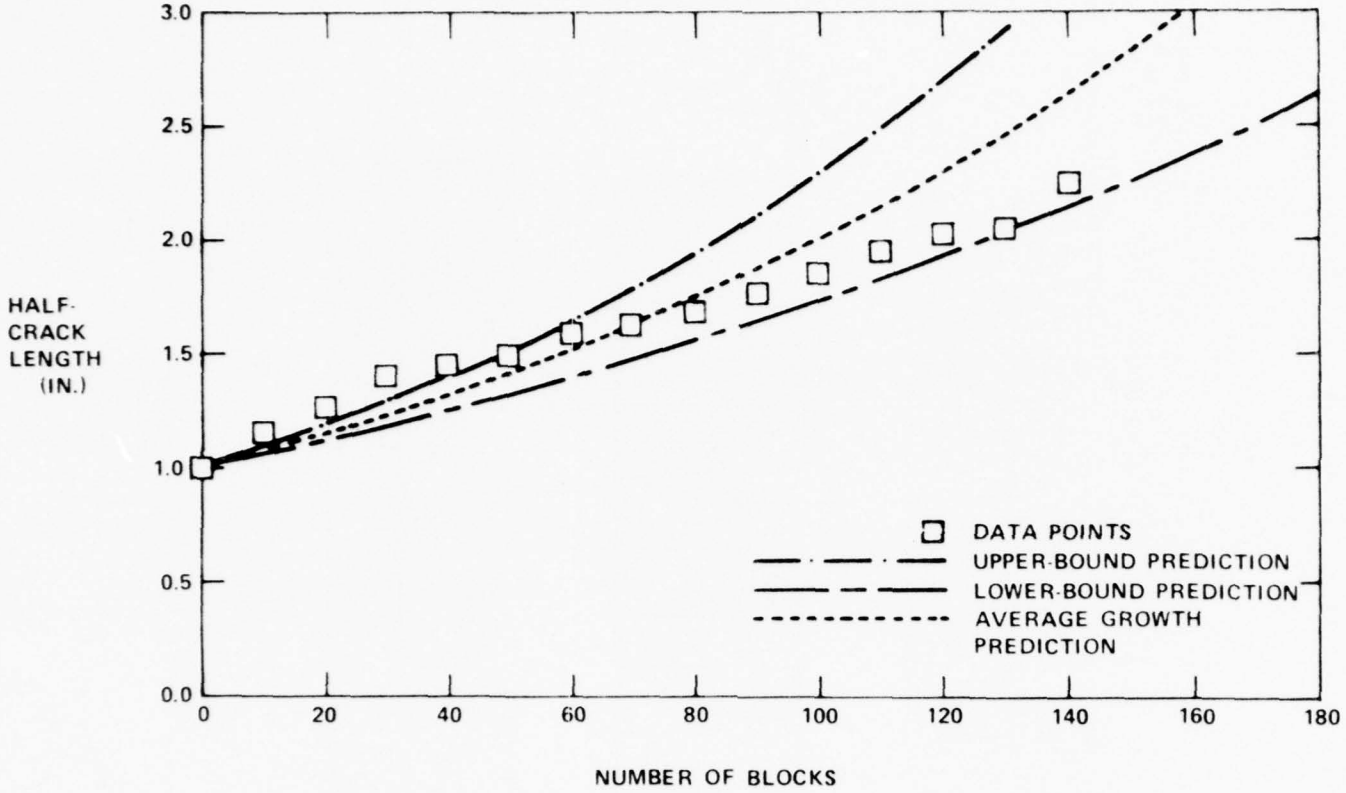

Figure 10 — Through-Crack Analyses for Box Beam 5, Crack 1

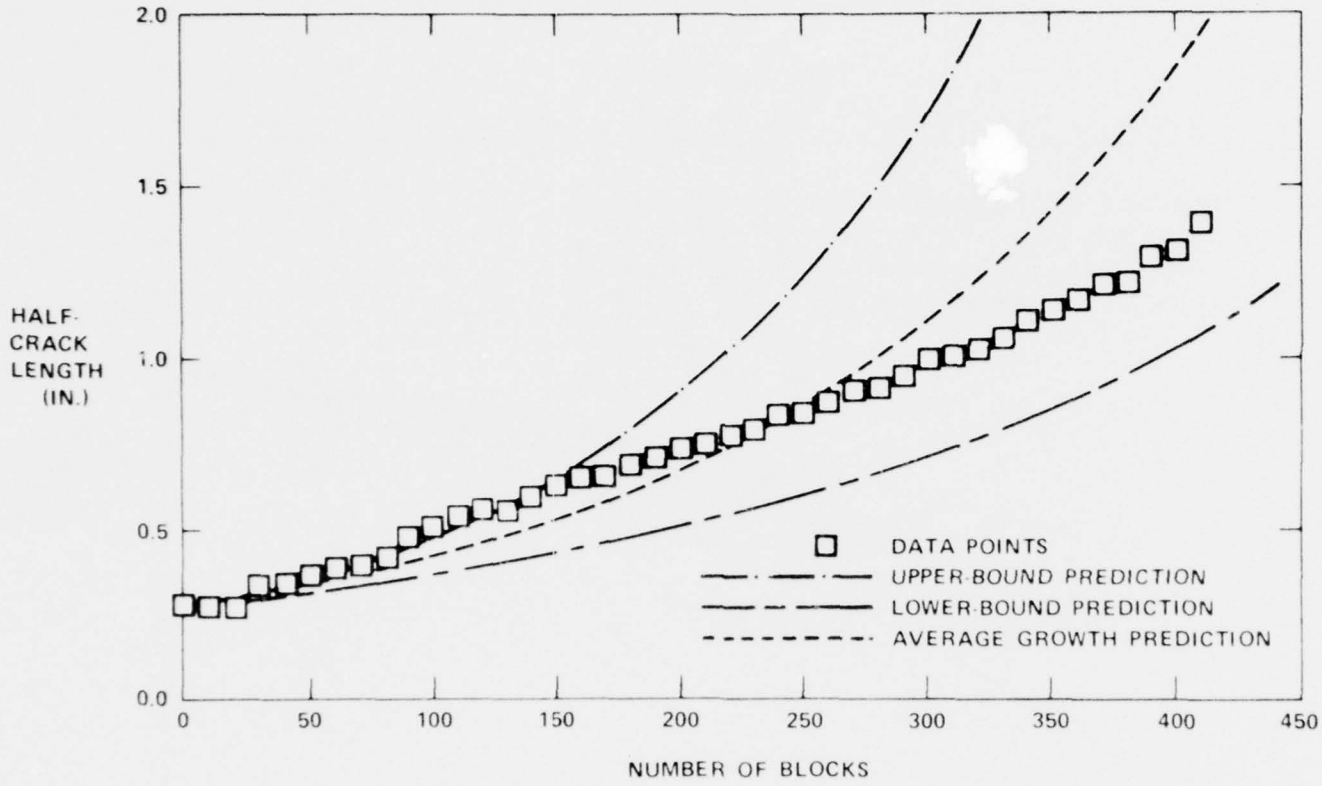

Figure 11 — Through-Crack Analyses for Box Beam 6, Crack 2

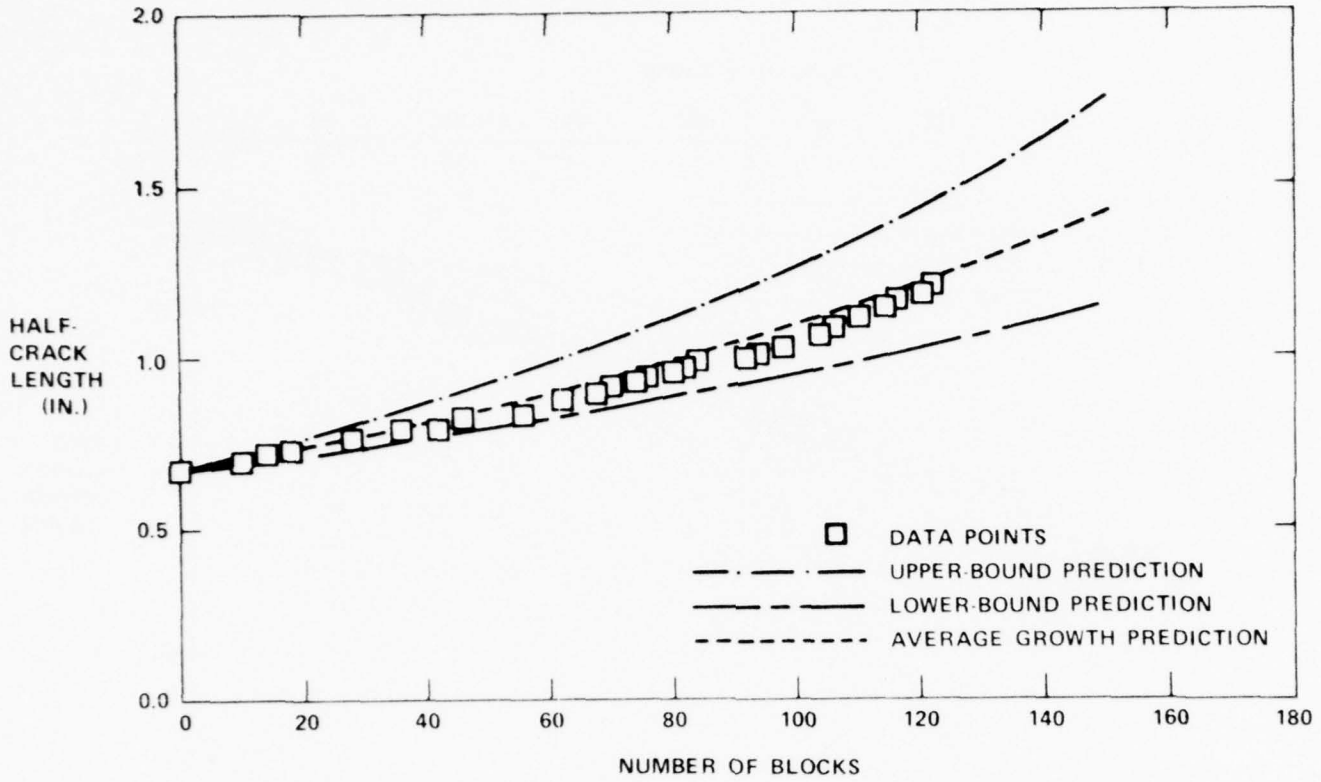

Figure 12 — Through-Crack Analyses for Box Beam 6, Crack 3

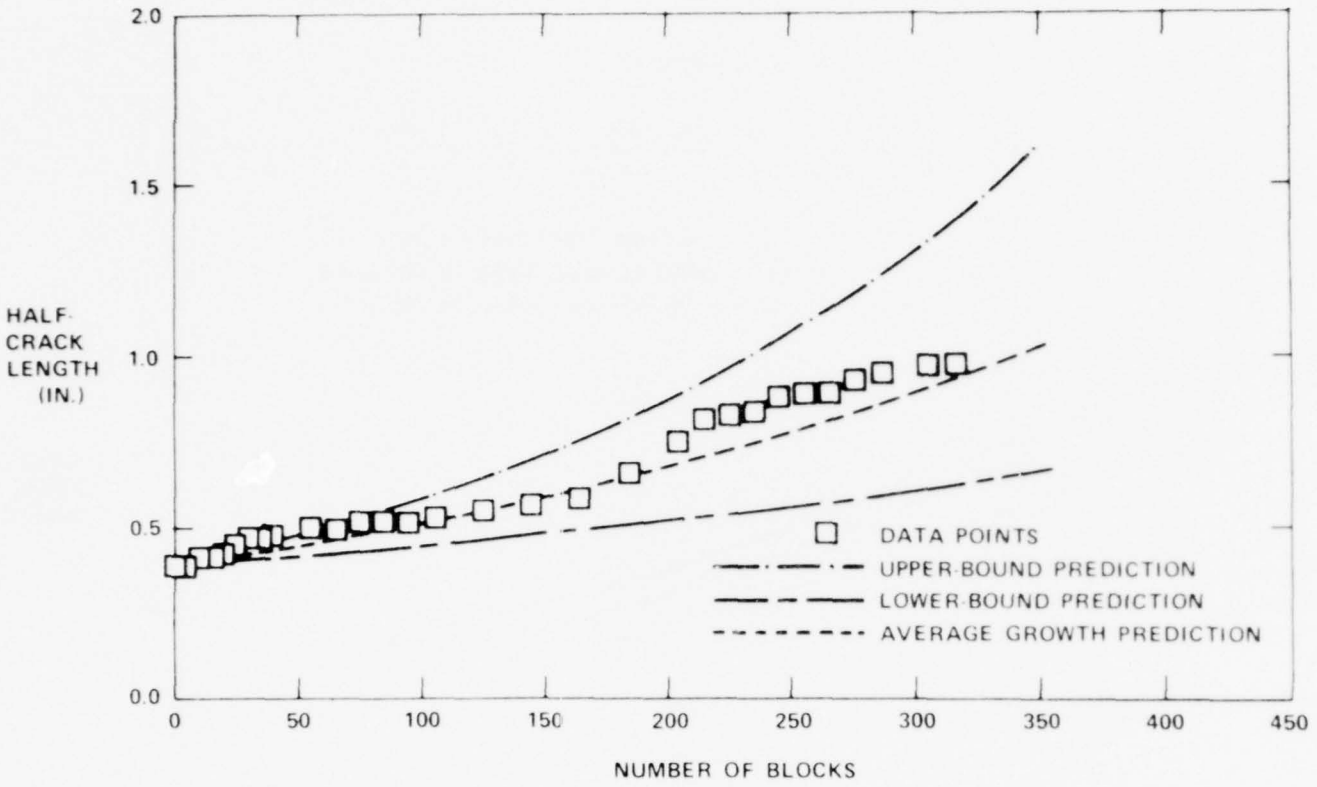

Figure 13 — Through-Crack Analyses for Box Beam 7

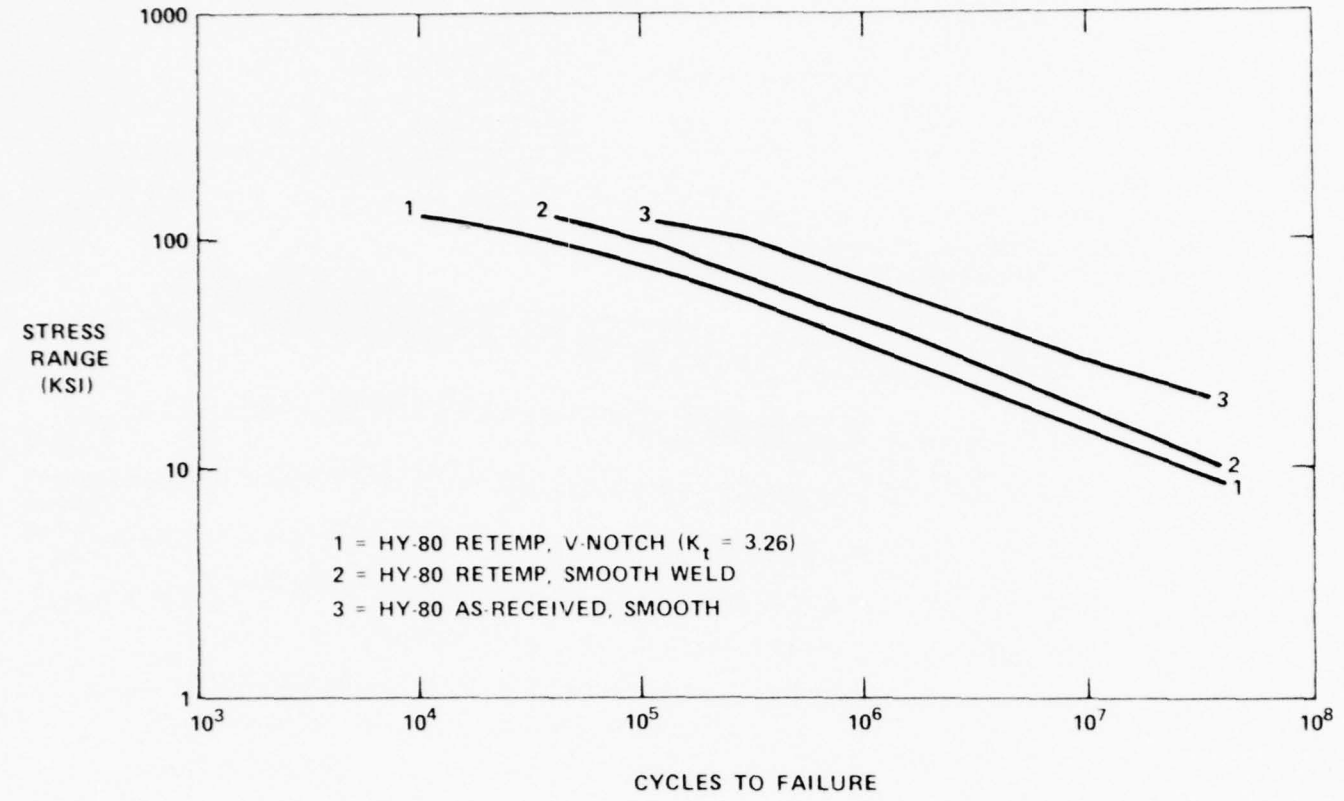

Figure 14 — Fatigue Data for HY-80 Steel in Saltwater

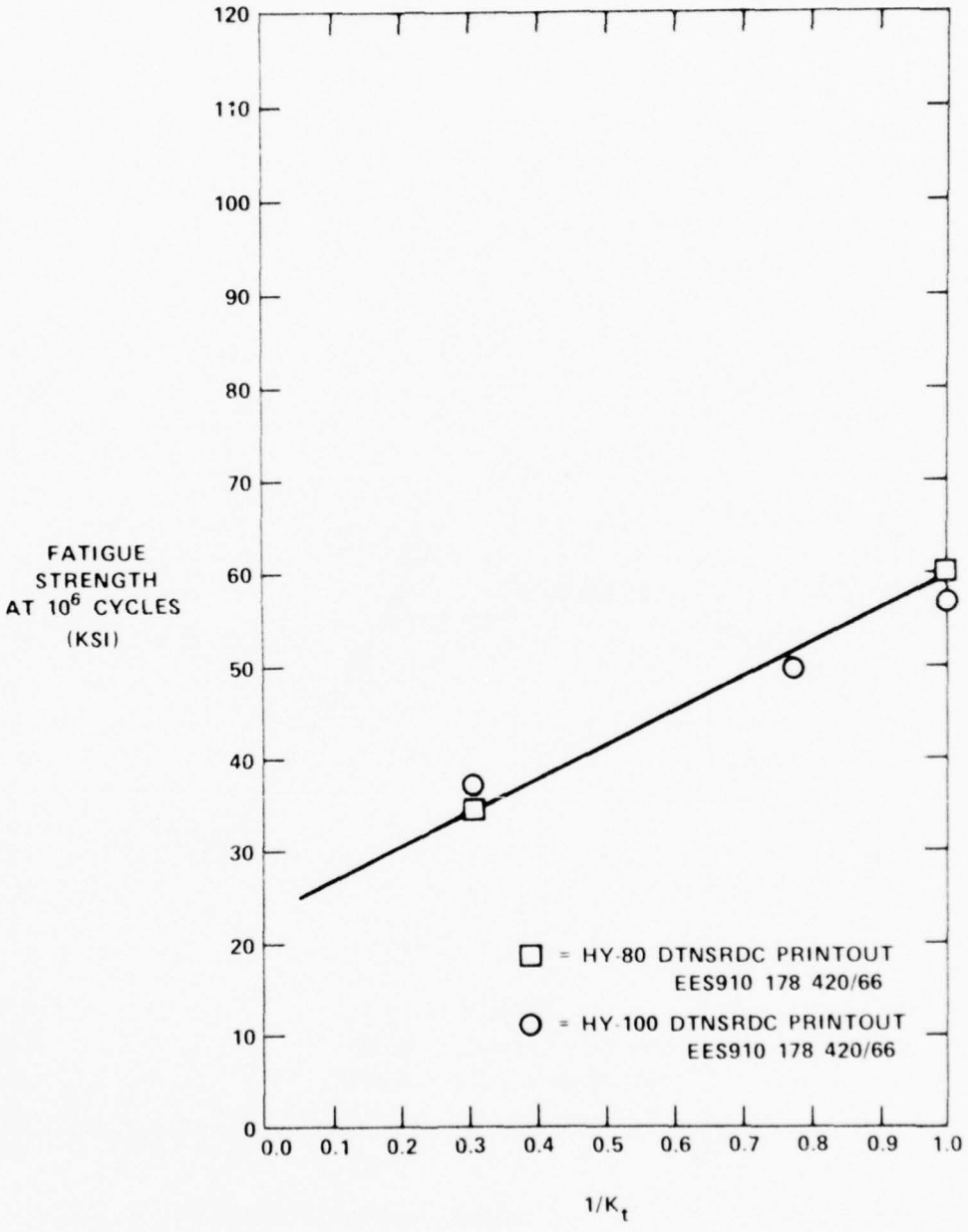

Figure 15 — Fatigue Strength versus $1/K_t$ for HY-80 Steel in Saltwater

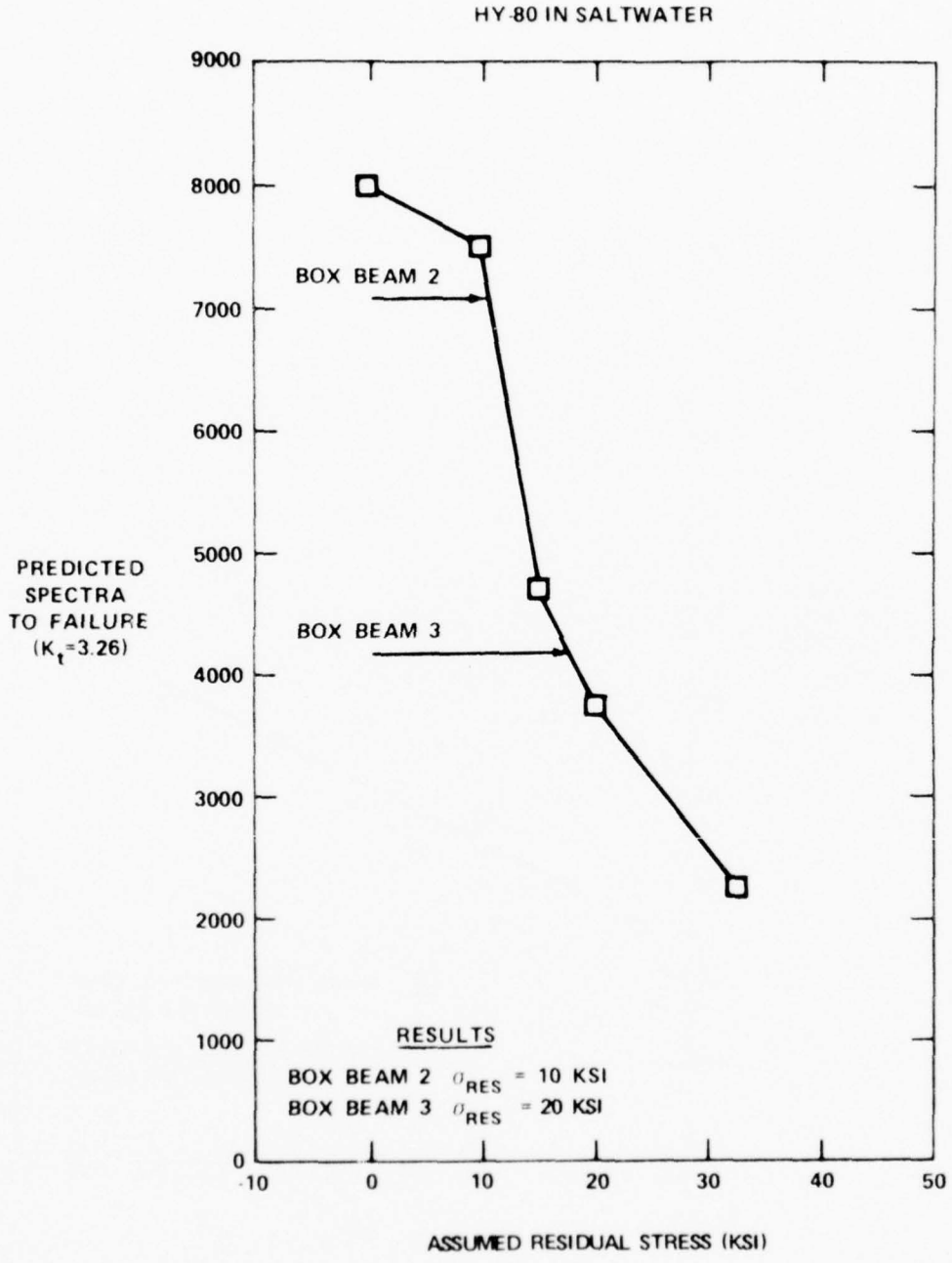

Figure 16 — Residual Stresses in Box Beams 2 and 3

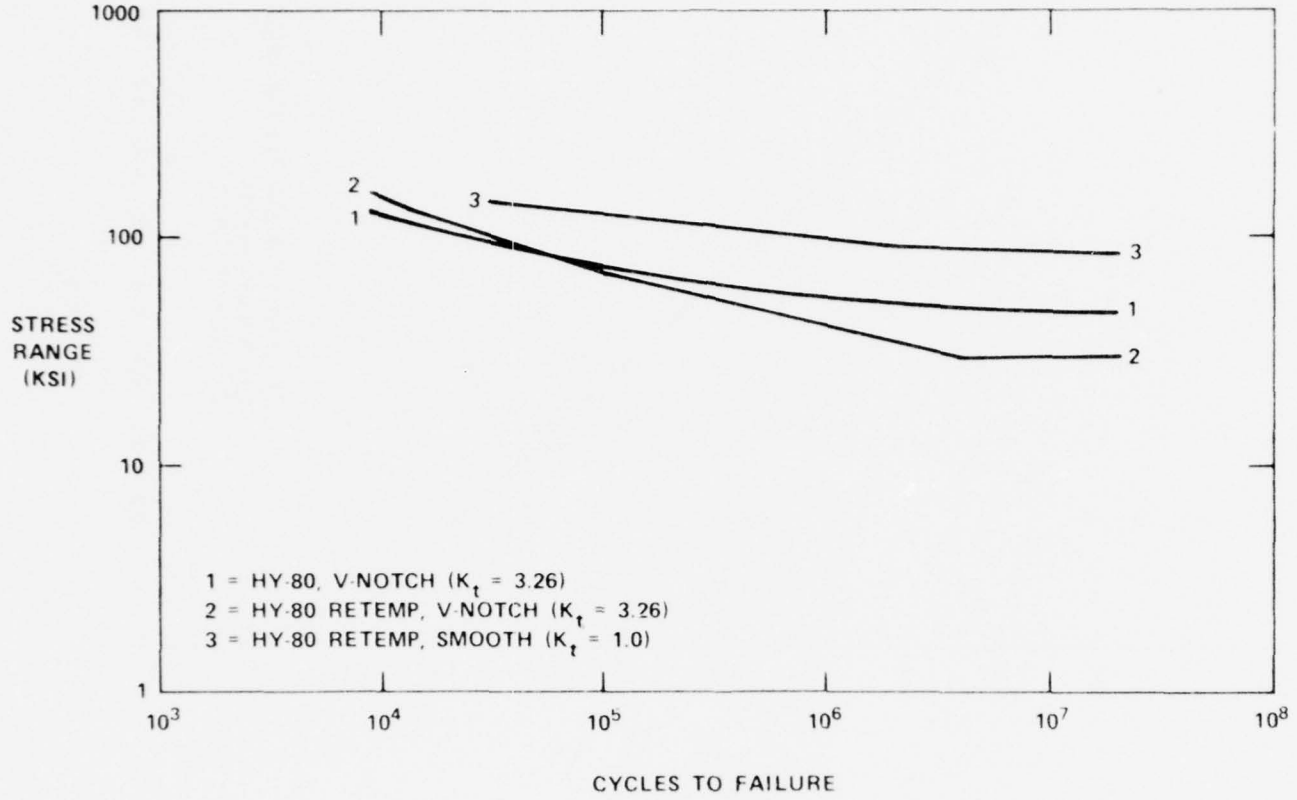

Figure 17 — Fatigue Data for HY-80 Steel in Air

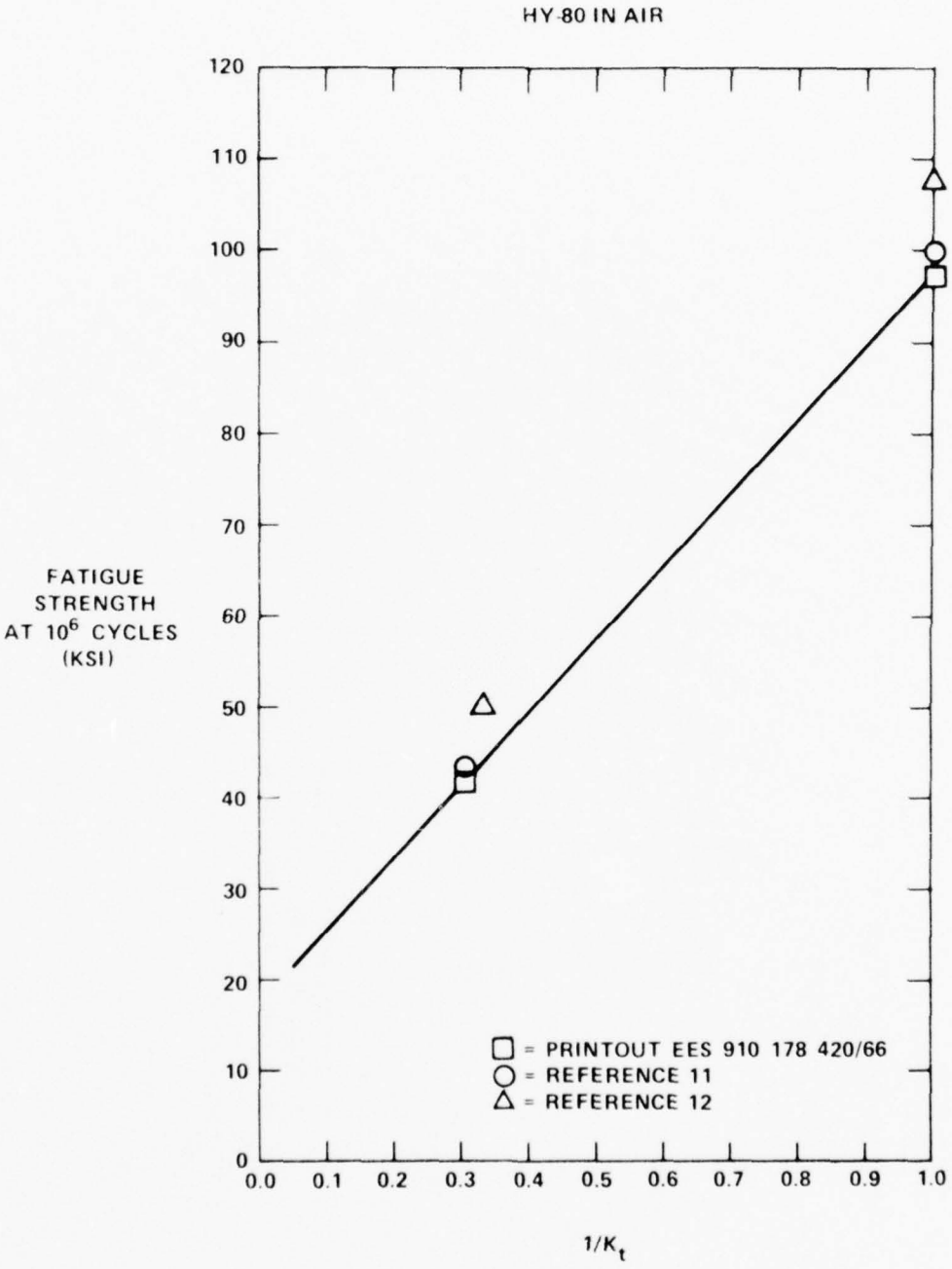

Figure 18 - Fatigue Strength versus $1/K_t$ for HY-80 Steel in Air

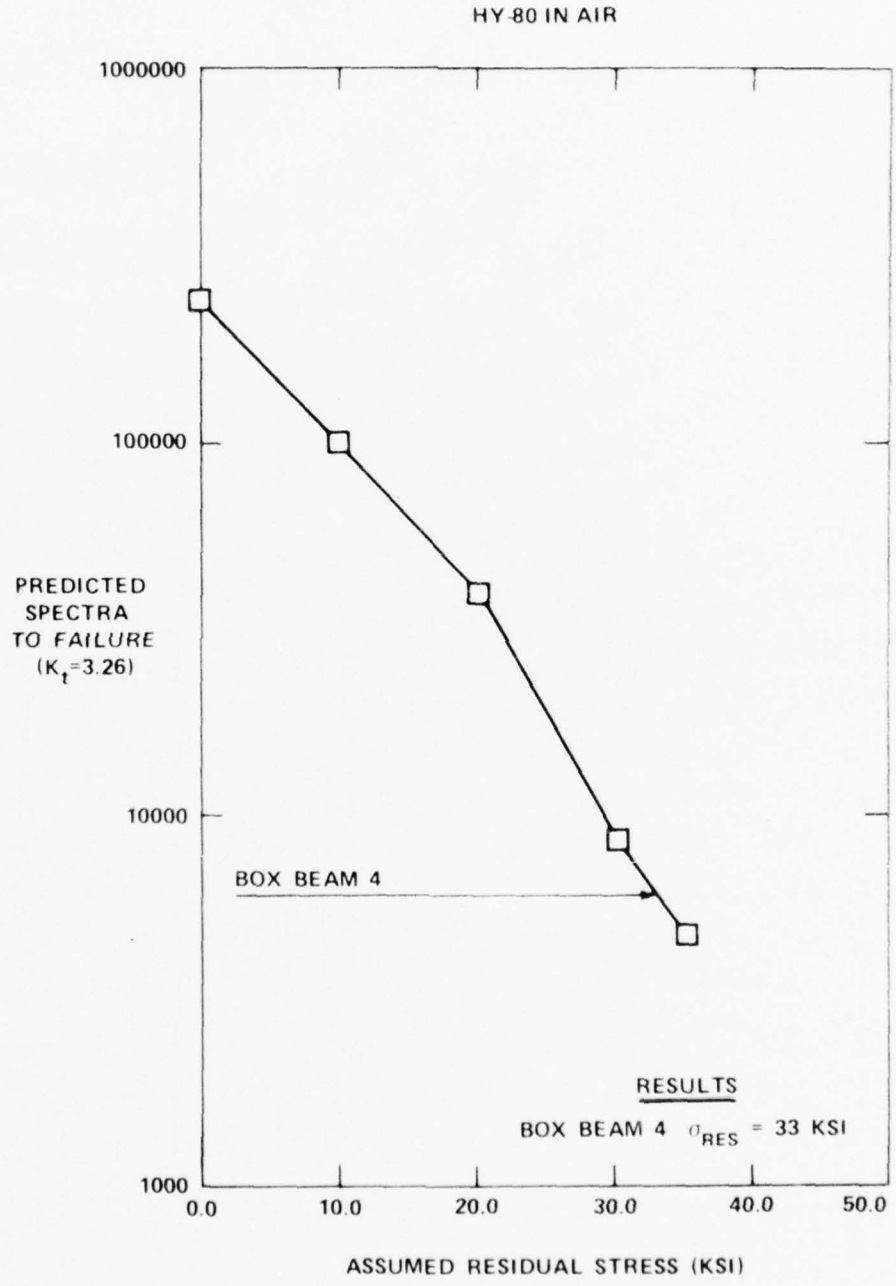

Figure 19 — Residual Stresses in Box Beam 4

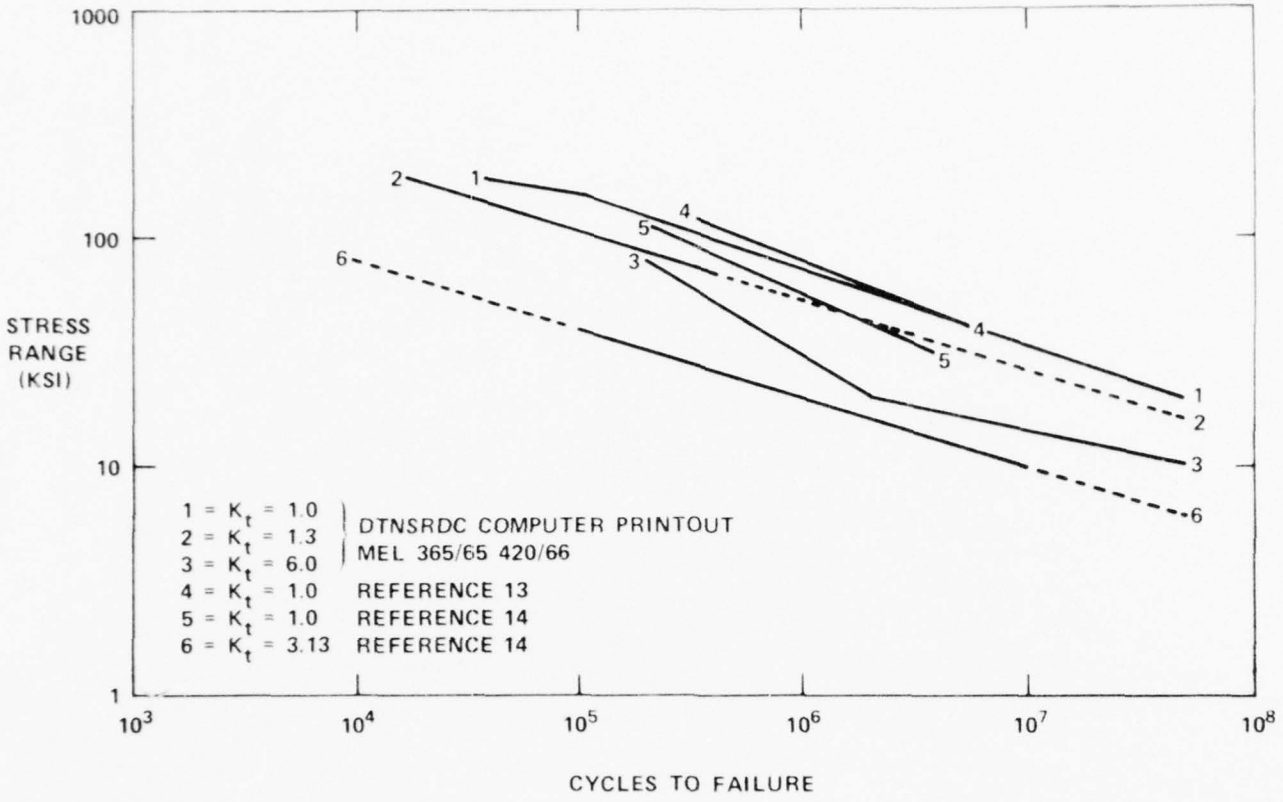

Figure 20 — Fatigue Data for HY-130 Steel in Saltwater

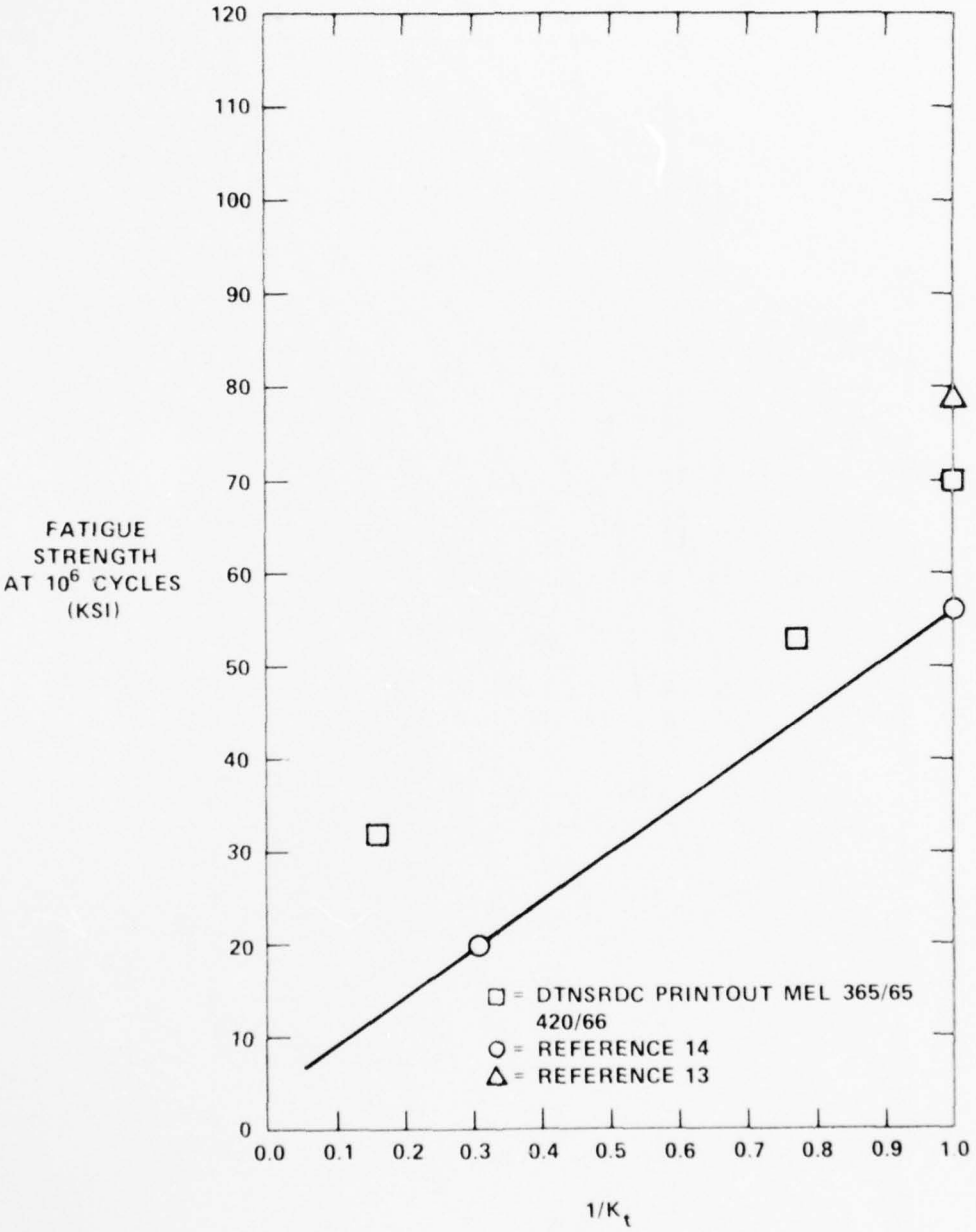

Figure 21 — Fatigue Strength versus $1/K_t$ for HY-130 Steel in Saltwater

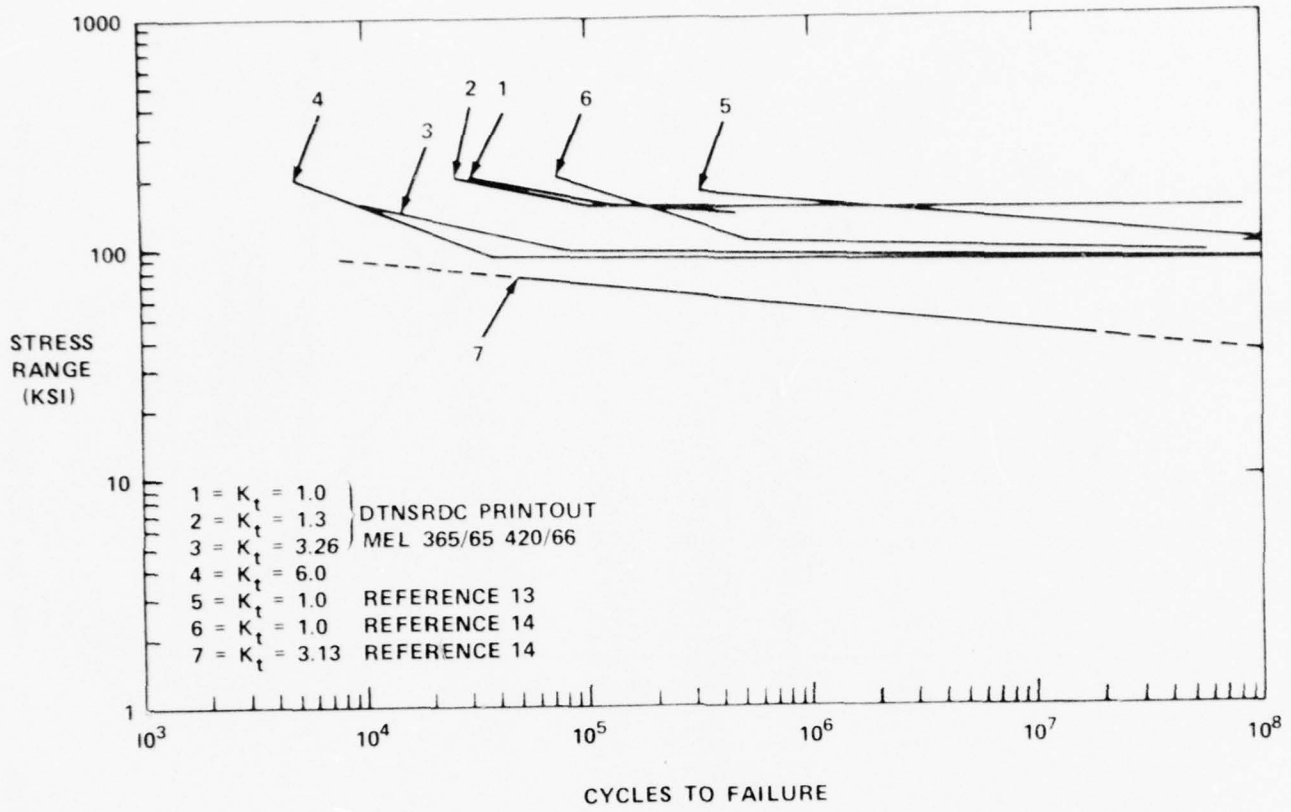

Figure 22 — Fatigue Data for HY-130 Steel in Air

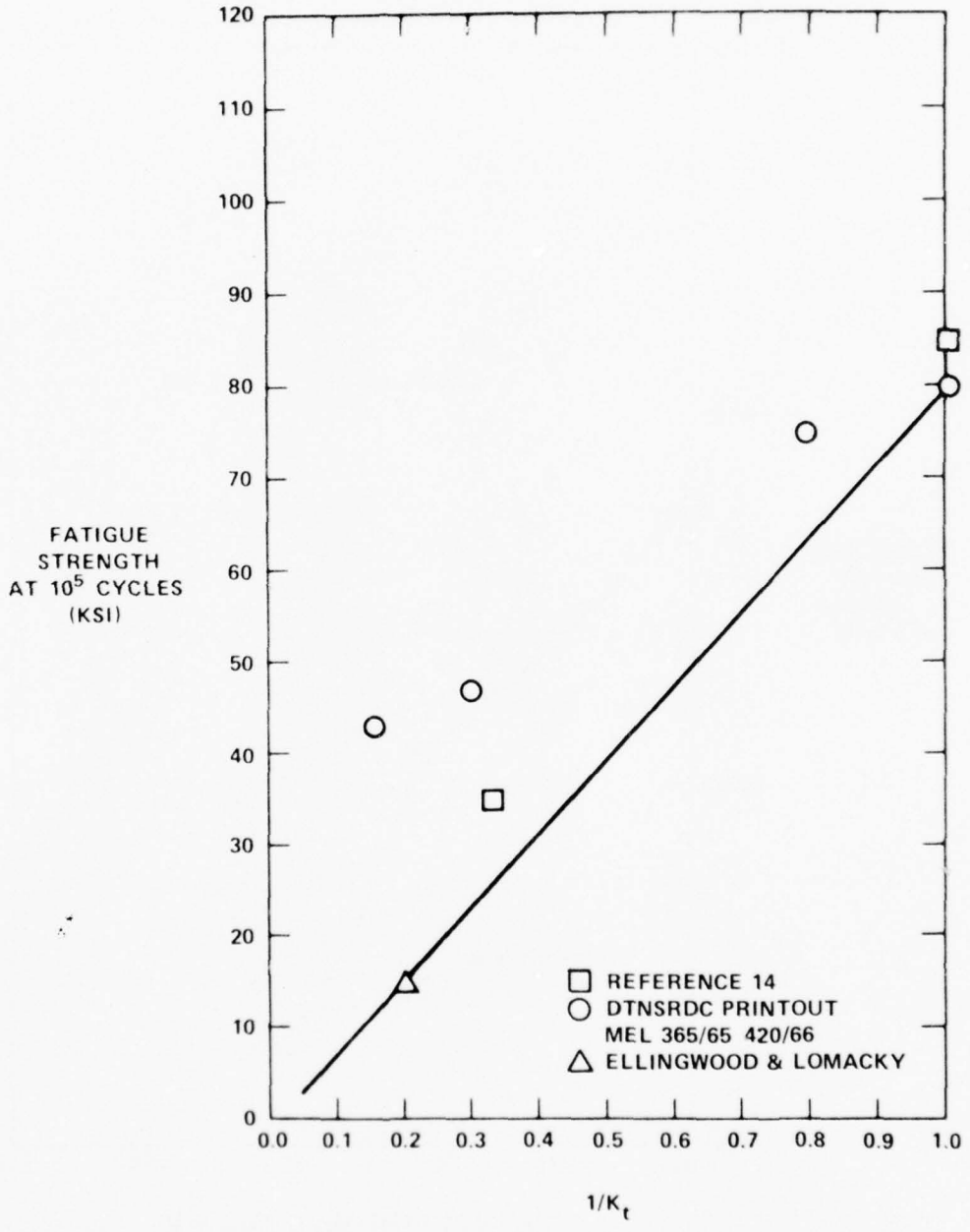

Figure 23 — Fatigue Strength versus $1/K_t$ for HY-130 Steel in Air

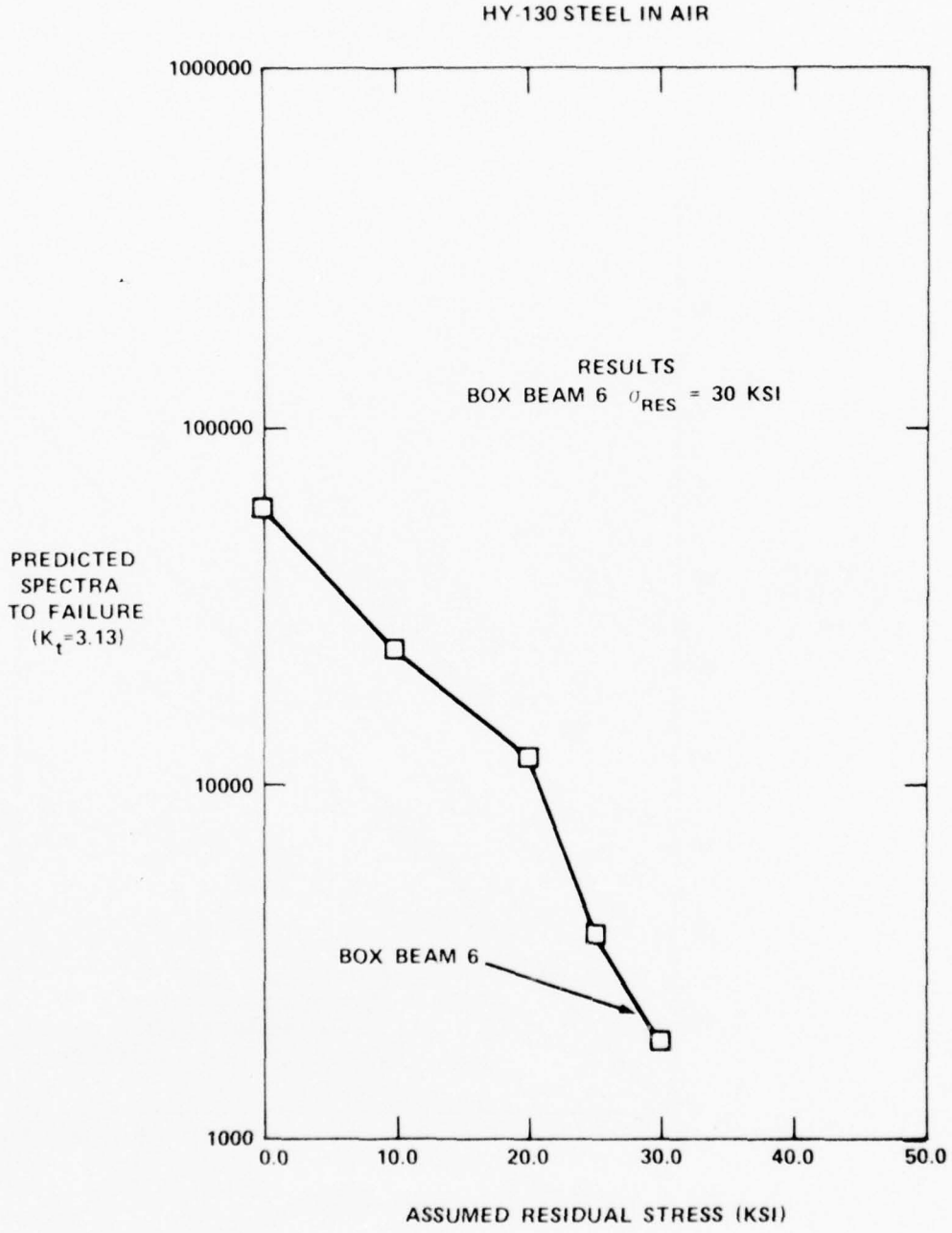

Figure 24 — Residual Stresses in Box Beam 6

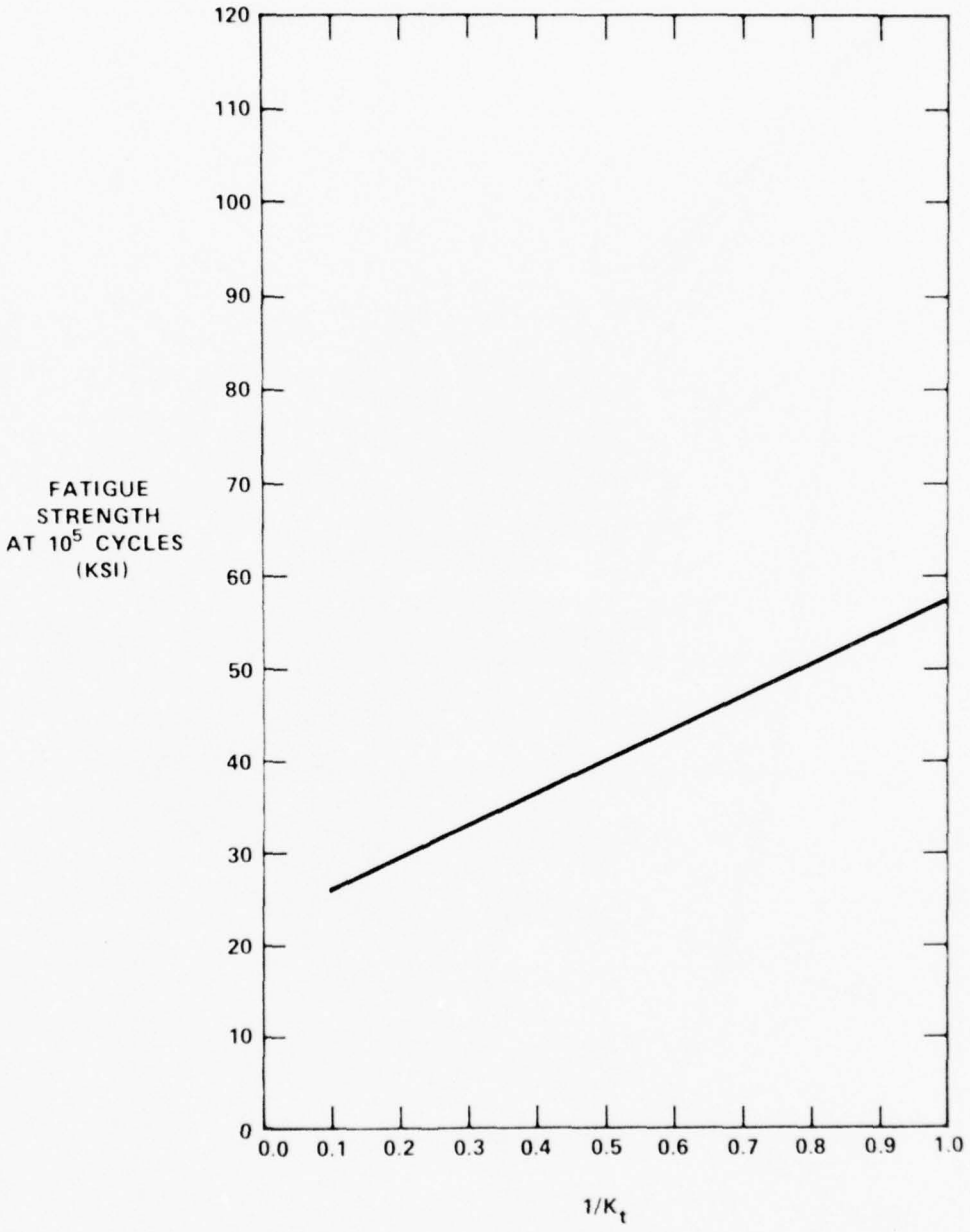

Figure 25 — Fatigue Strength versus $1/K_t$ for 17-4PH Steel in Saltwater

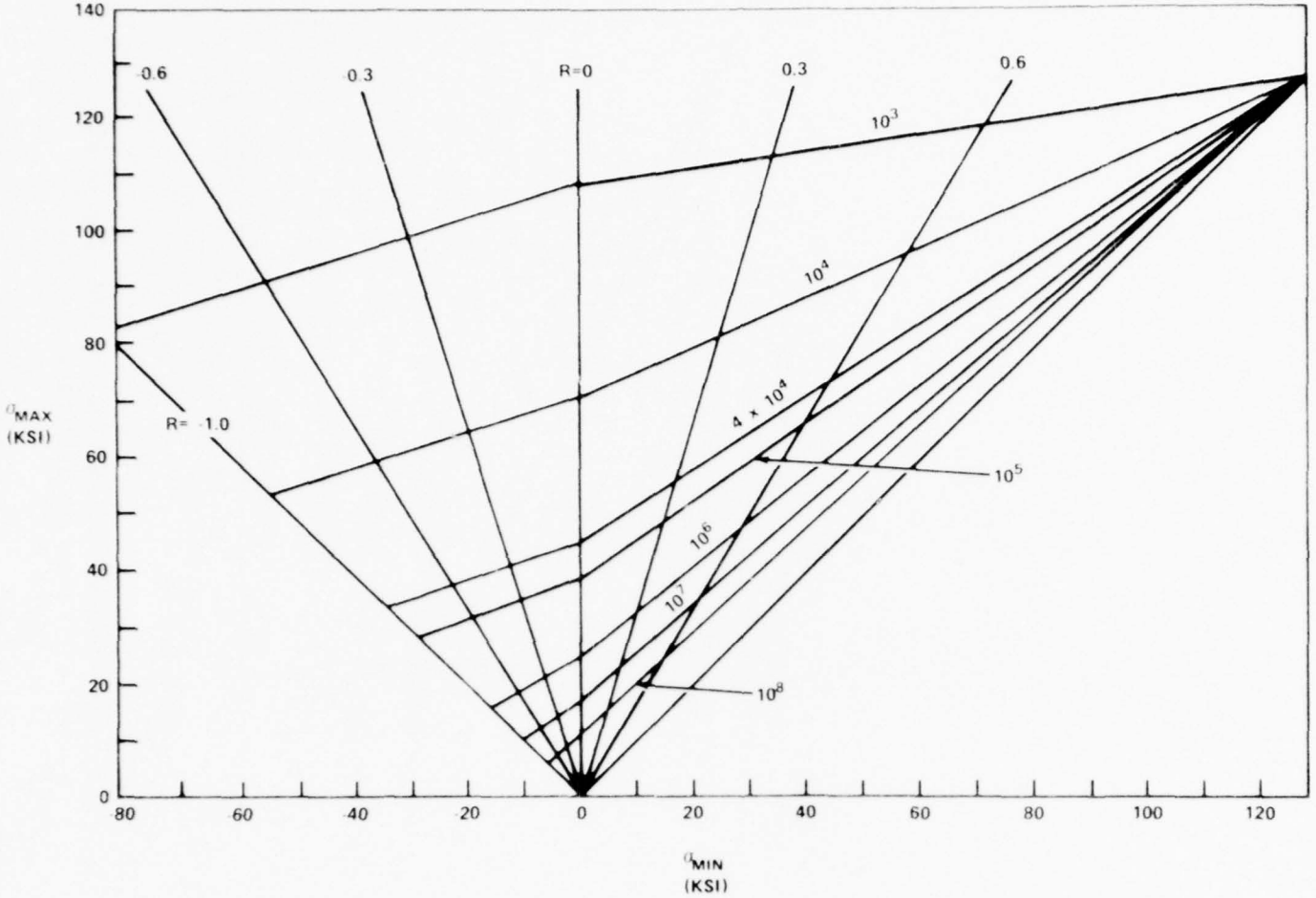

Figure 26 — Constant-Life Diagram for 17-4PH Steel (K_t=2)

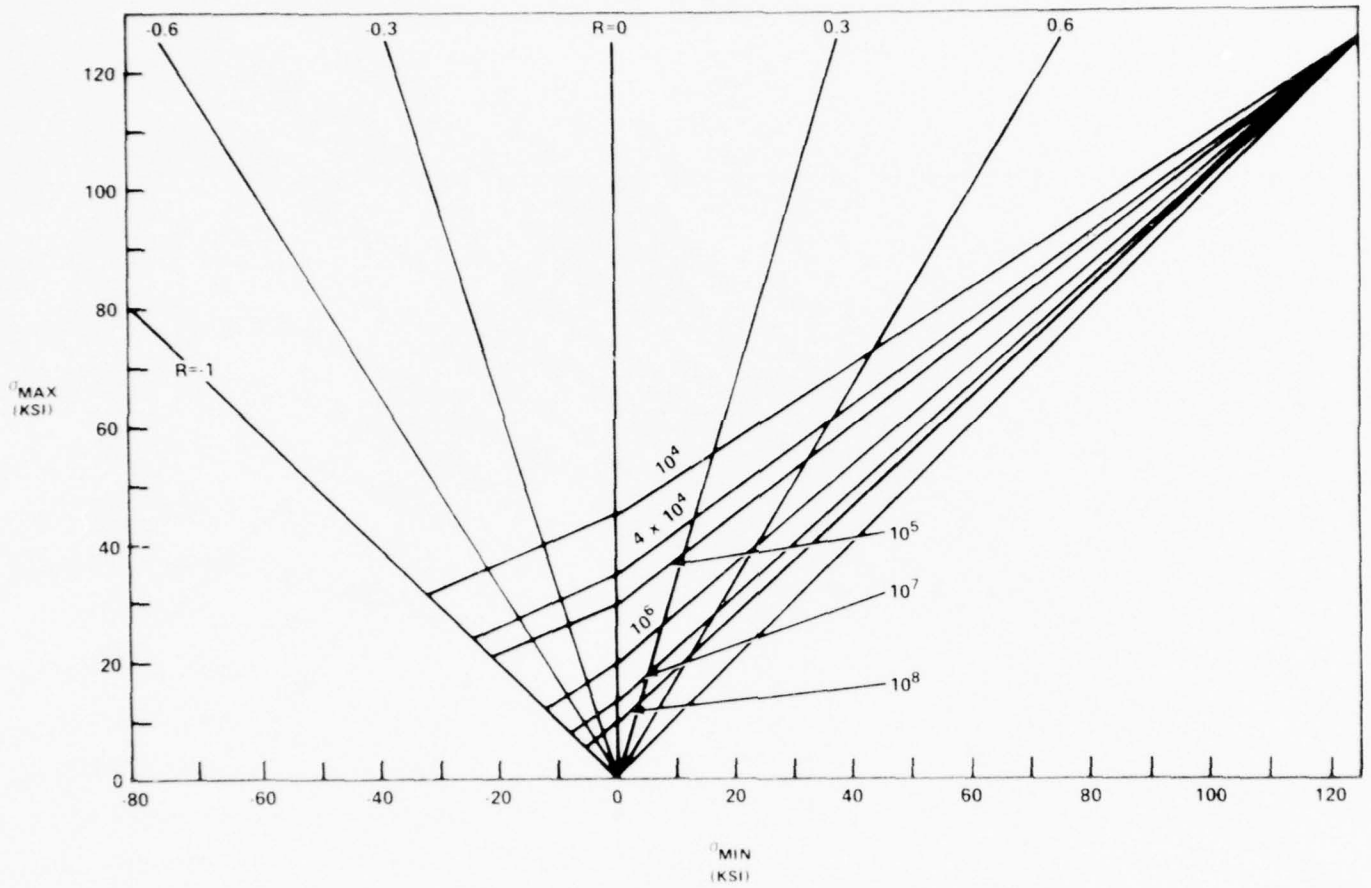

Figure 27 — Constant-Life Diagram for 17-4PH Steel (K_t=3)

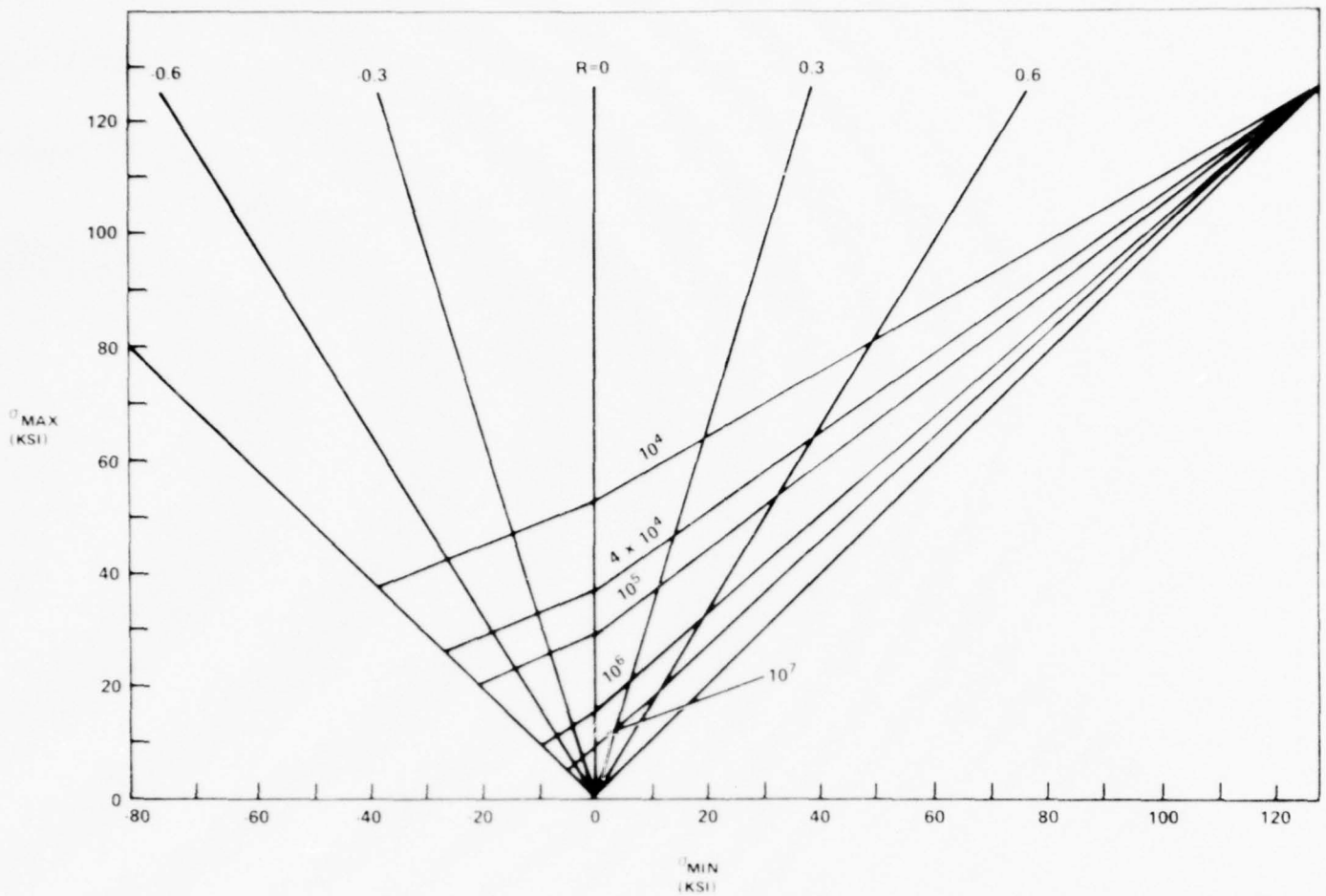

Figure 28 — Constant-Life Diagram for 17-4PH Steel (K_t=4)

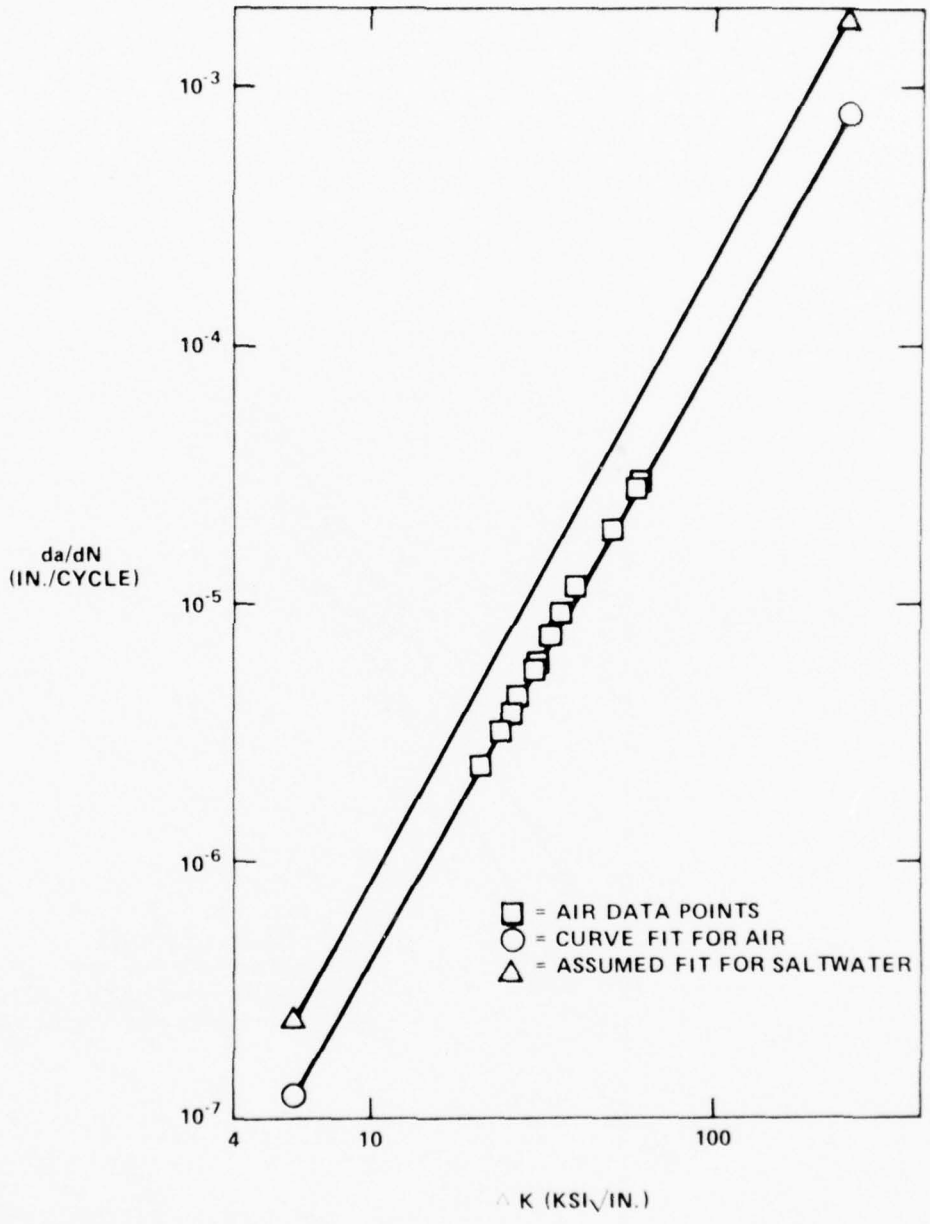

Figure 29 — Crack-Growth Rates on HY-80 Steel

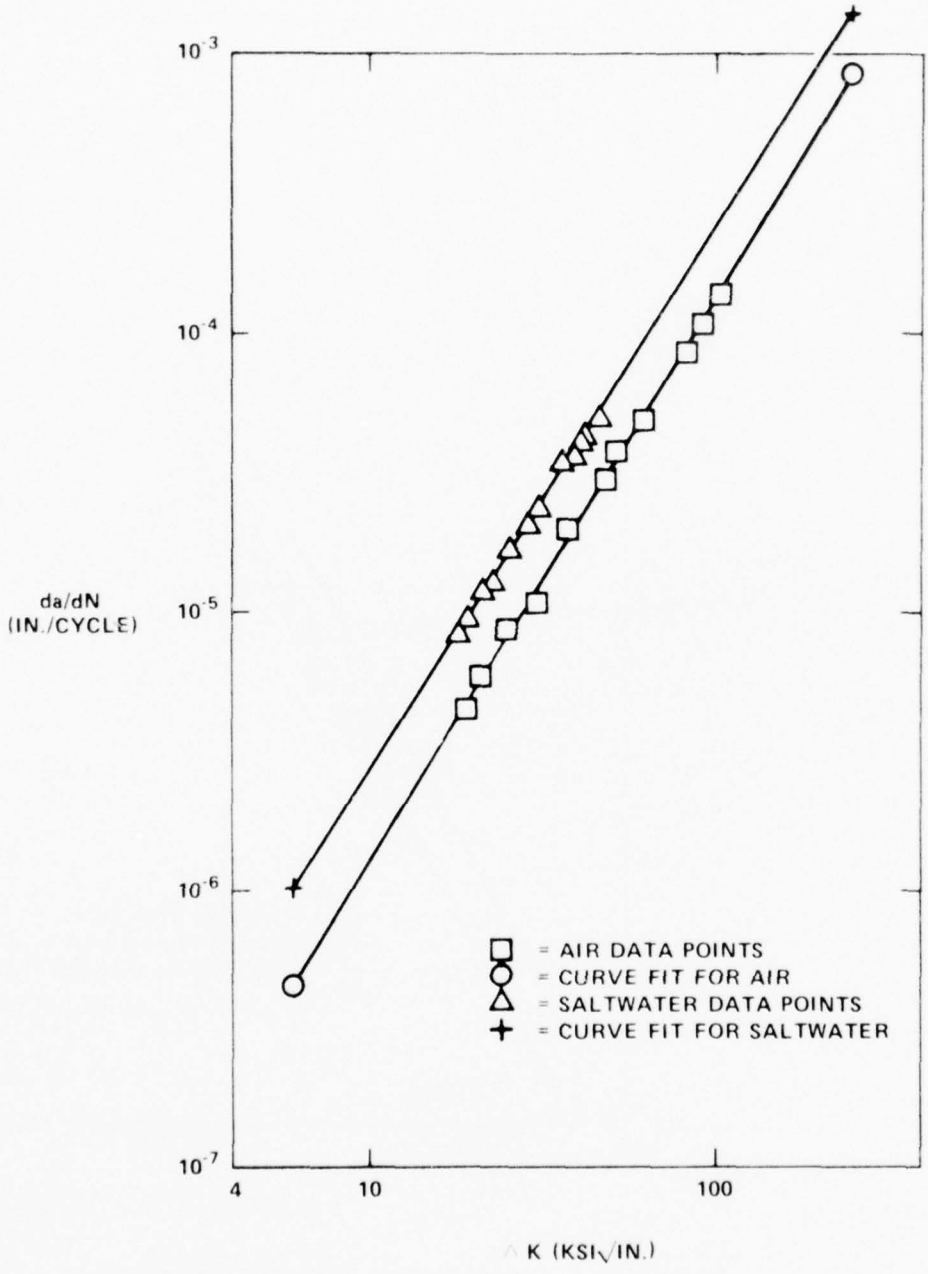

Figure 30 — Crack-Growth Rates on HY-130 Steel

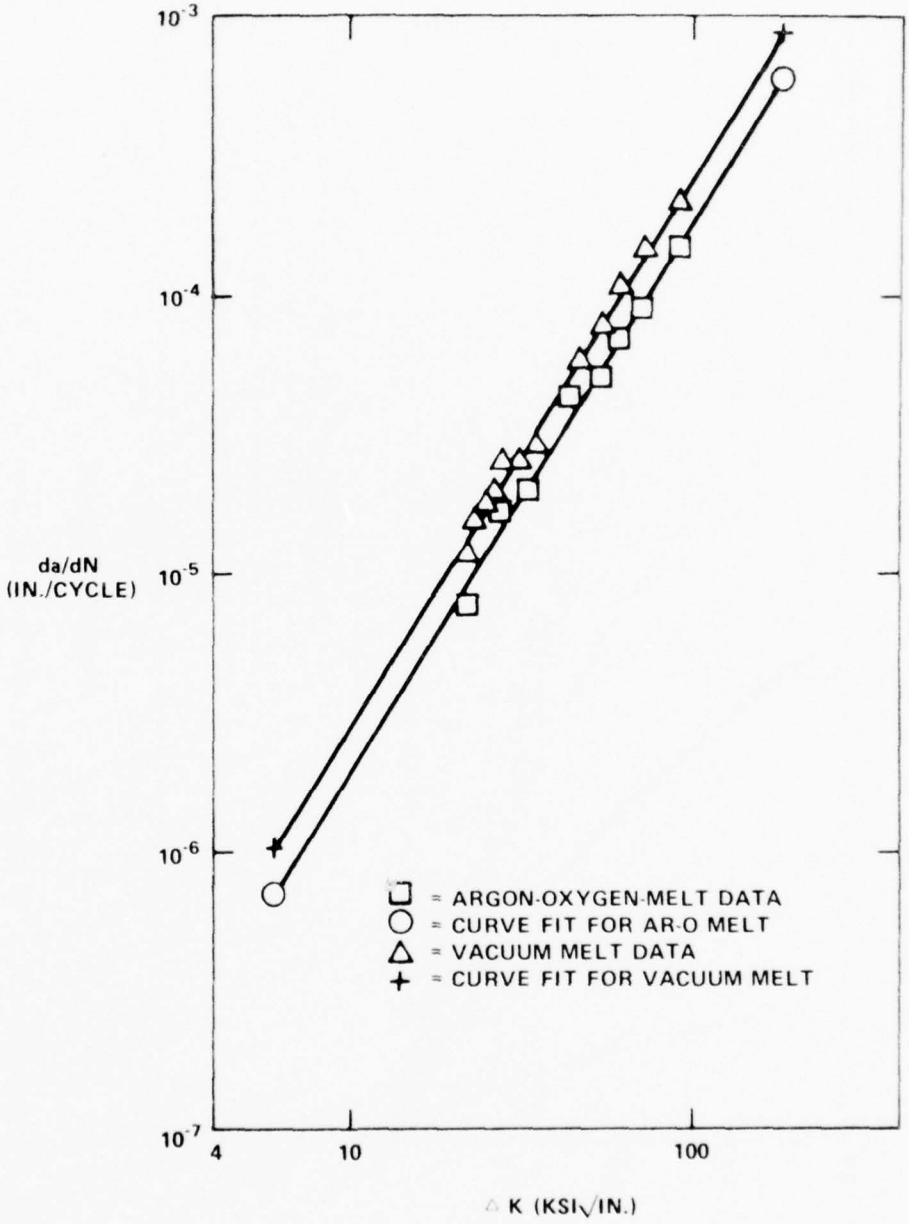

Figure 31 — Crack-Growth Rates on 17-4PH H1050 Steel in Saltwater

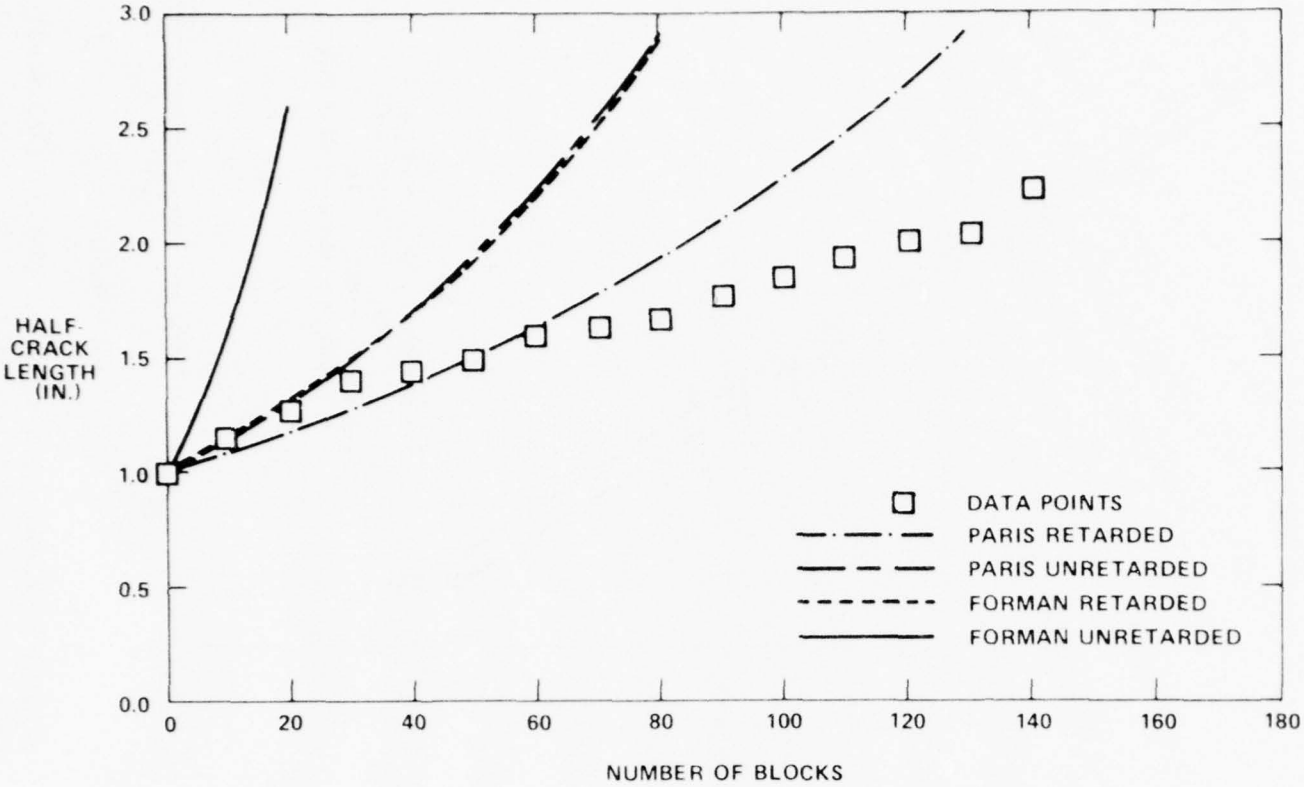

Figure 32 — Through-Crack Analyses for Box Beam 5, Crack 1

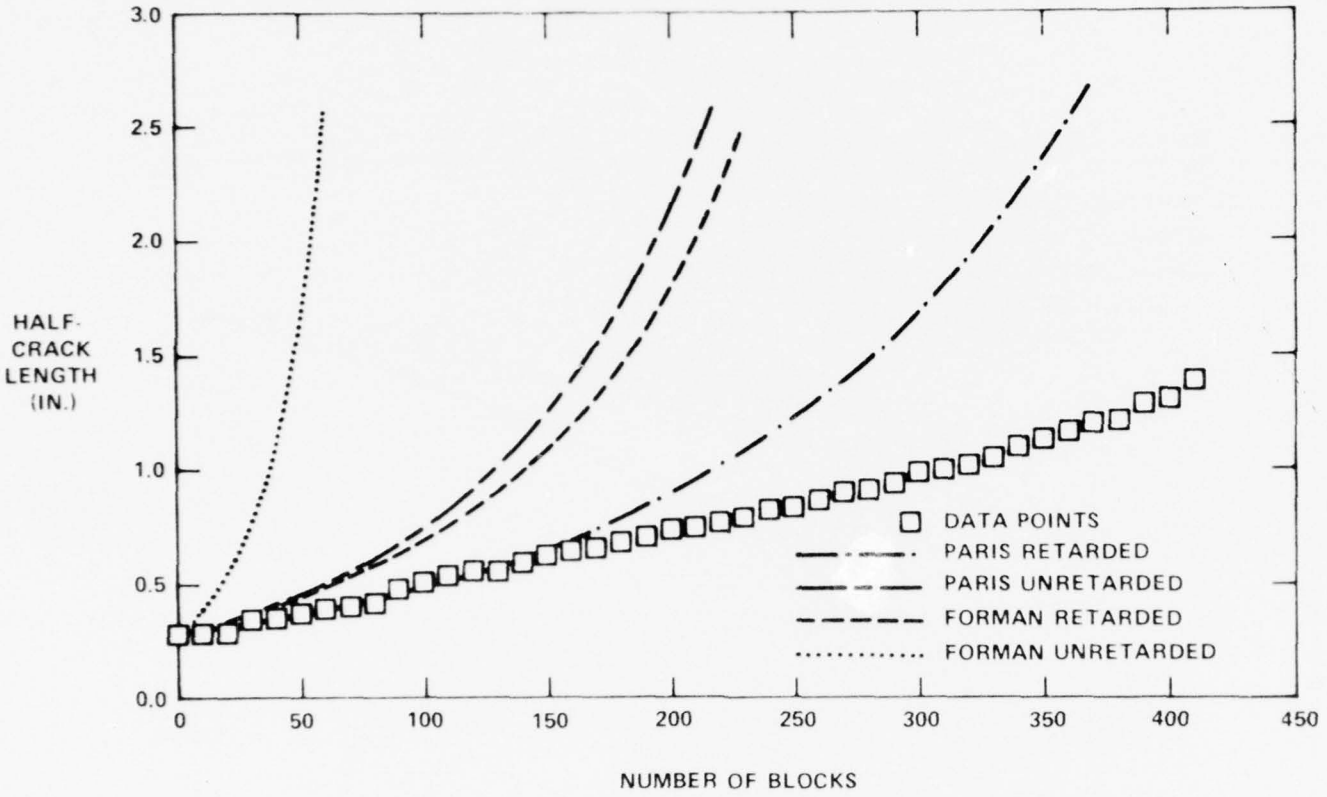

Figure 33 — Through-Crack Analyses for Box Beam 6, Crack 2

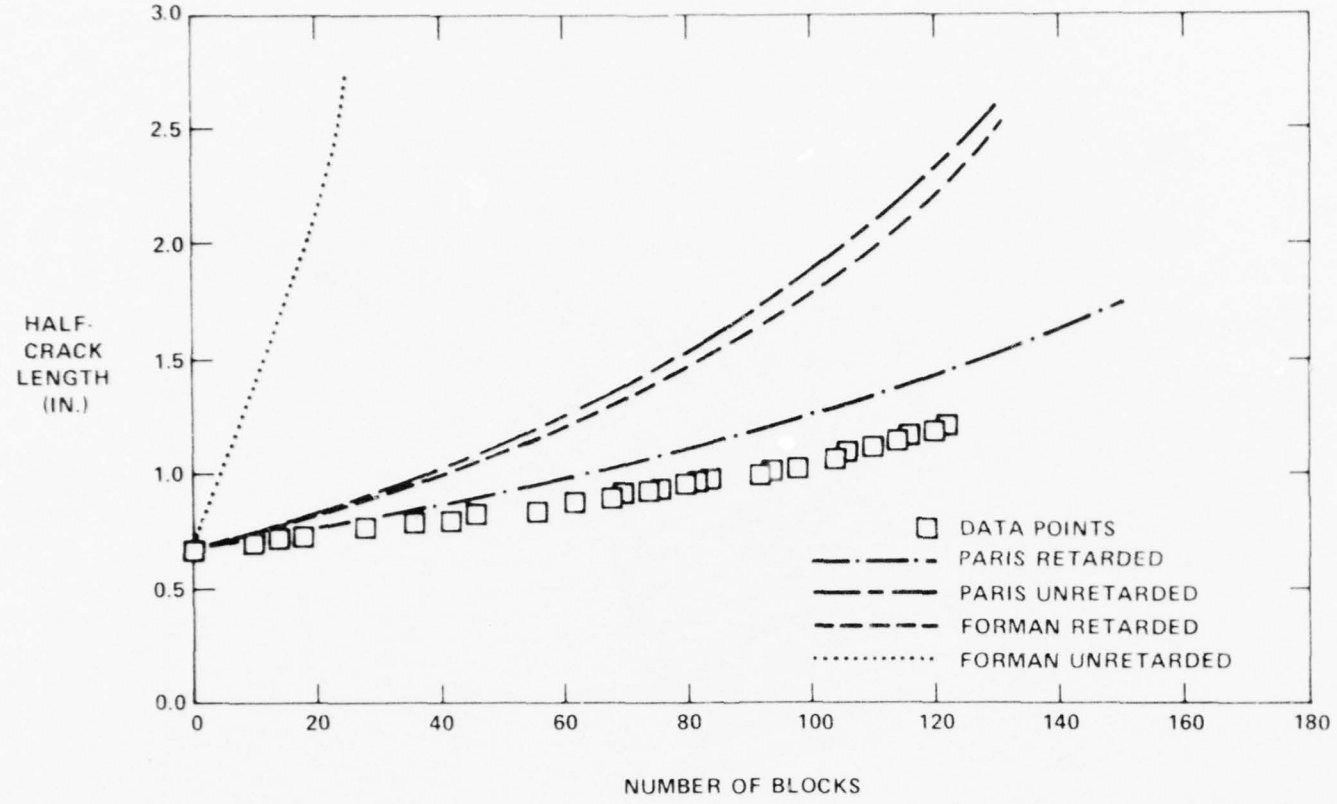

Figure 34 — Through-Crack Analyses for Box Beam 6, Crack 3

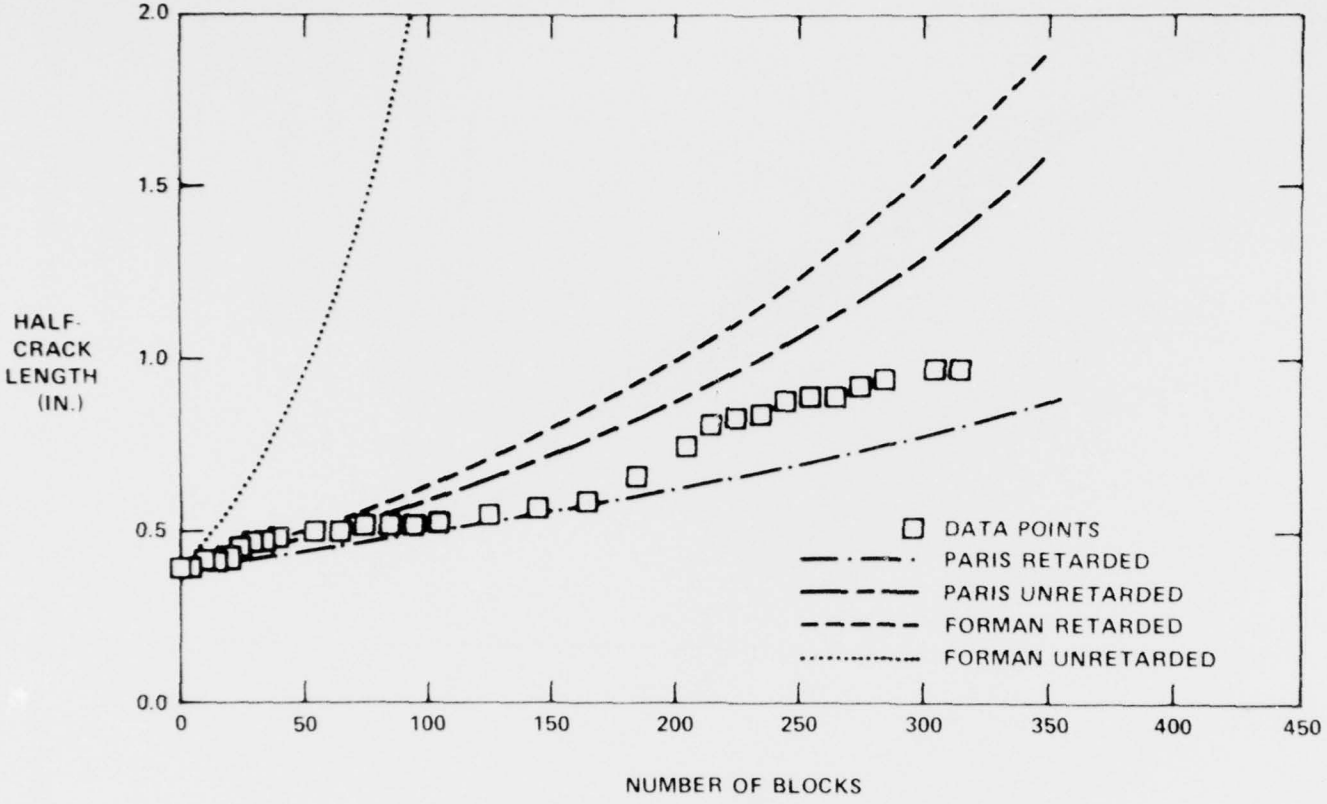

Figure 35 — Through-Crack Analyses for Box Beam 7

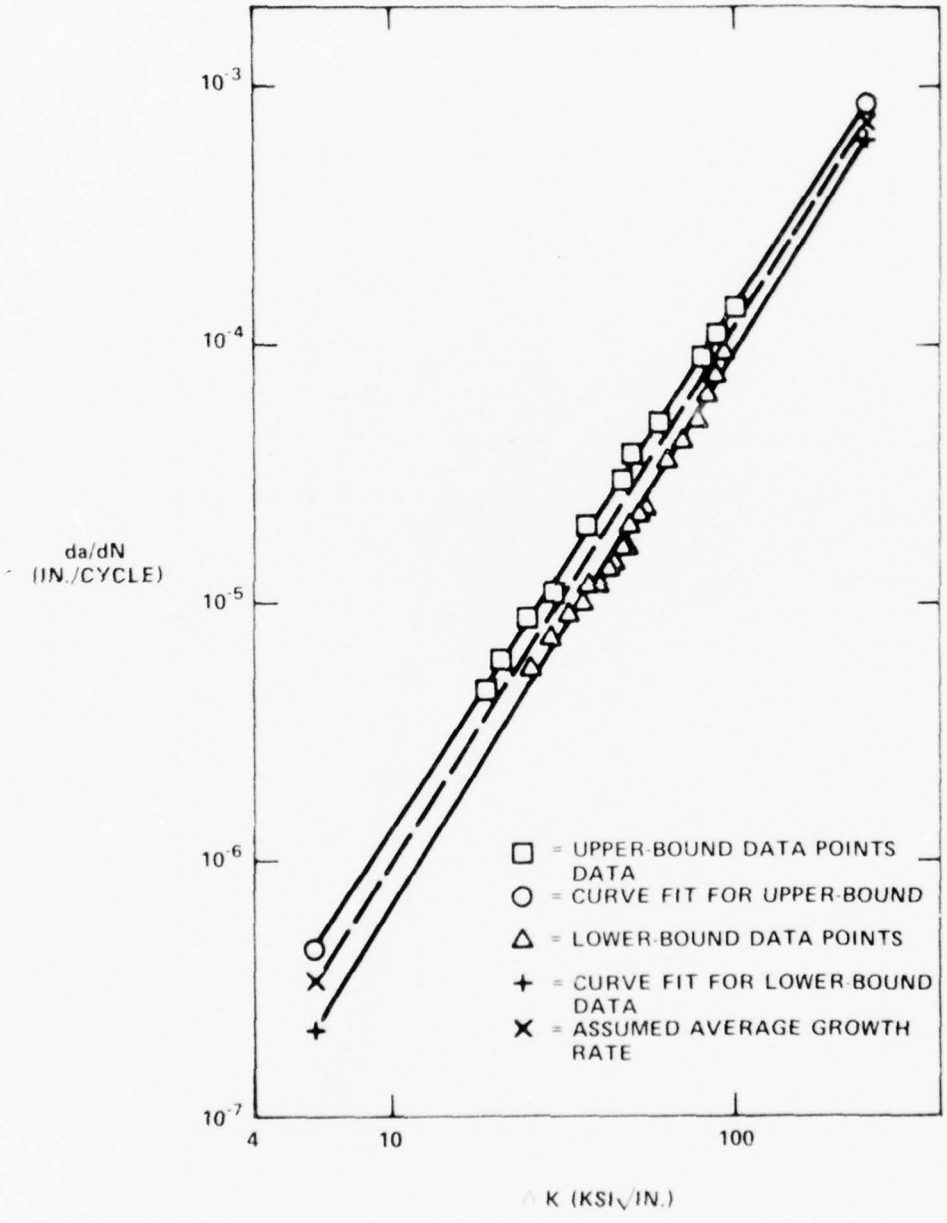

Figure 36 — Crack-Growth Rates in Air for HY-130 Steel

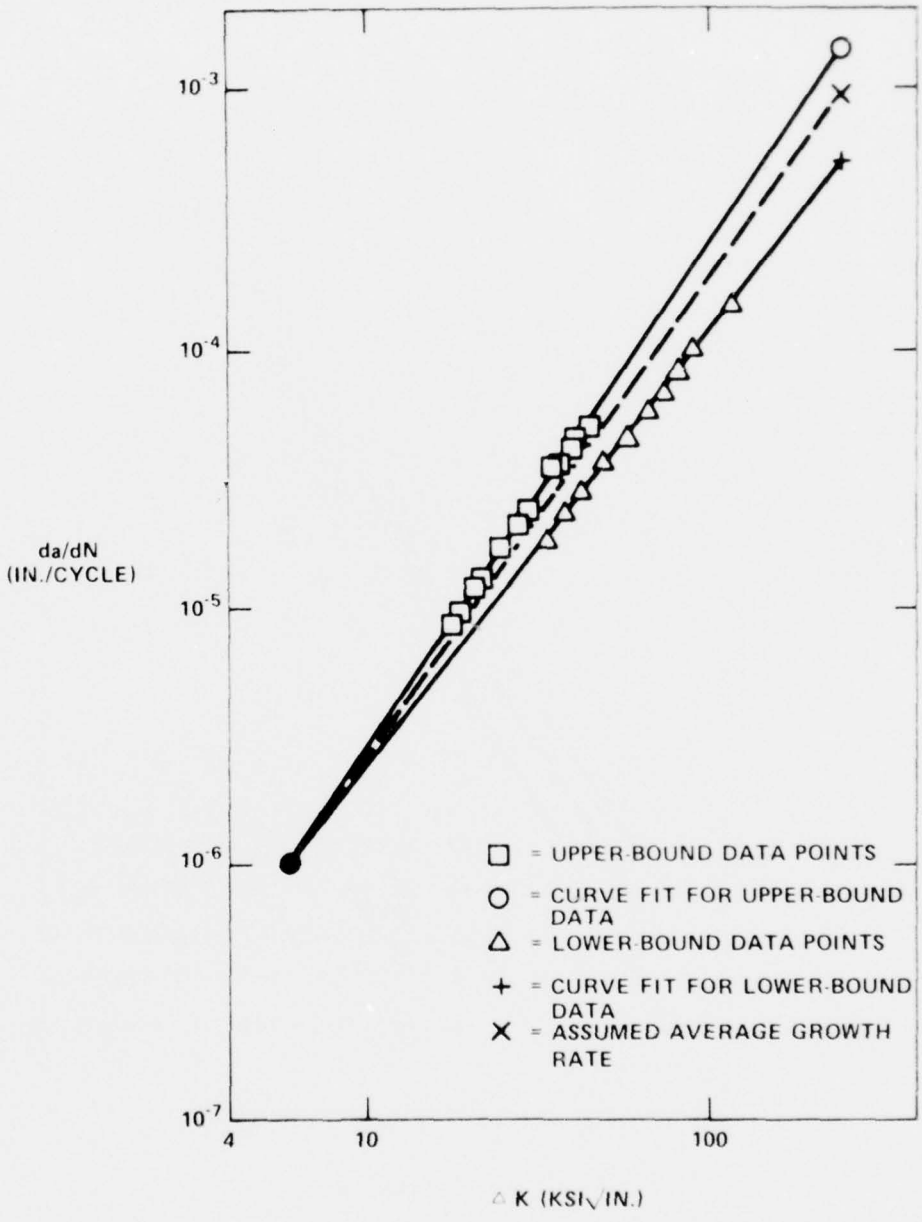

Figure 37 — Crack-Growth Rates in Saltwater for HY-130 Steel

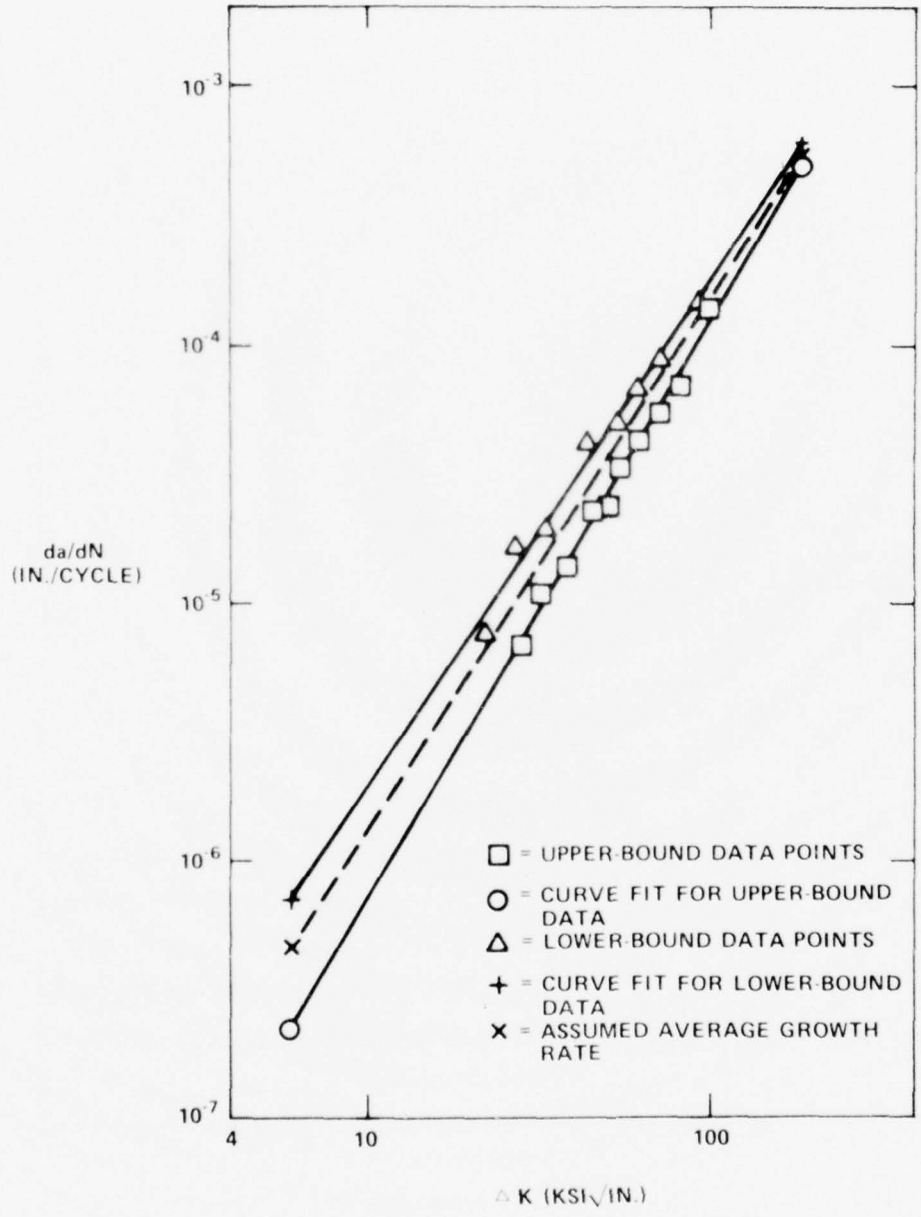

Figure 38 — Crack-Growth Rates in Saltwater for 17-4PH Steel

TABLE 1 — MATERIAL, CLOSEOUT CONFIGURATION, AND TEST ENVIRONMENT FOR BOX BEAMS 1 THROUGH 8

Box Beam	Material	Configuration	Environment
1	HY-80	Slot	Air
2	HY-80	Slot	Saltwater
3	HY-80	Patch	Saltwater
4	HY-80	Slot	Air
5	HY-130	Patch	Saltwater
6	HY-130	Slot	Air
7	17-4PH	Tee	Saltwater
8	17-4PH	Patch	Saltwater

TABLE 2 — DETERMINATION OF MAXIMUM STRESSES FOR BOX BEAMS 2 THROUGH 8

Box Beam	Material	Maximum Load kips	Measured Sensitivity psi/kips	σ_{Max}* ksi
2	HY-80	62.73	840	52.69
3	HY-80	62.73	840	52.69
4	HY-80	62.73	840	52.69
5	HY-130	80.5	1030	82.915
6	HY-130	75.5	1020	77.01
7	17-4PH	52.5	1160	60.90
8	17-4PH	65	1250	81.25

* σ_{Max} = Maximum load times measured sensitivity.

TABLE 3 — STRESS SPECTRA FOR BOX BEAMS 2 THROUGH 8

N-Cycles	Box Beam									
	2,3,4 HY-80		5 HY-130		6 HY-130		7 17-4PH		8 17-4PH	
	σ_{Max}	σ_{Min}	σ_{Max}	σ_{Min}	σ_{Max}	σ_{Min}	σ_{Max}	σ_{Min}	σ_{Max}	σ_{Min}
1	23.18	0.00	36.48	0.00	33.88	0.00	26.79	0.00	35.75	0.00
544	27.82	18.54	43.78	29.18	40.66	27.10	32.15	21.43	42.90	28.60
1	23.18	-23.18	36.48	-36.48	33.88	-33.88	26.79	-26.79	35.75	-35.75
312	33.30	22.20	52.41	34.93	48.67	32.45	38.50	25.66	51.35	34.23
1	52.69	27.75	82.915	43.67	77.01	40.56	60.90	32.08	81.25	42.79
69	38.79	25.85	61.04	40.68	56.69	37.79	44.84	29.88	59.81	39.87
1	52.69	27.75	82.915	43.67	77.01	40.56	60.90	32.08	81.25	42.79
69	38.79	25.85	61.04	40.68	56.69	37.79	44.84	29.88	59.81	39.87
1	52.69	27.75	82.915	43.67	77.01	40.56	60.90	32.08	81.25	42.79

Note: All stress in ksi (kilopounds per square inch).

TABLE 4 — FIRST-FAILURE LOCATIONS FOR BOX BEAMS 2 THROUGH 8

Box Beam	Material	Test Environment	First-Failure Location
2	HY-80	Saltwater	Cracking in slot welds, 7080 blocks.
3	HY-80	Saltwater	Crack in butt weld, 4170 blocks.
4	HY-80	Air	Crack in slot weld, 6260 blocks.
5	HY-130	Saltwater	Two cracks in butt weld, 996 blocks.
6	HY-130	Air	Crack in slot weld, 1857 blocks.*
7	17-4PH	Saltwater	Crack in T-weld, 3051 blocks.
8	17-4PH	Saltwater	Crack in toe of fillet of internal transverse stiffener, 1226 blocks.

*First failure of box beam 6 was due to peening of a final fillet weld pass. This procedure is normally not allowed for HY-130. The next failure occurred at 2146 blocks.

TABLE 5 — EQUIVALENT STRESS SPECTRA FOR BOX BEAMS 2 THROUGH 8

N--	Equivalent Fully Reversed Stress Range of Box Beams R=-1 in ksi				
Cycles	2,3,4	5	6	7	8
544	11.98	19.50	17.44	13.62	18.48
312	15.20	25.00	22.10	17.22	23.48
138	18.86	31.34	27.40	21.26	29.12
1	46.36	72.96	67.76	53.58	71.50
3	40.72	69.56	59.38	45.68	63.32
1	29.57	47.31	43.16	33.90	45.64

TABLE 6 — COMPARISONS OF PREDICTED FATIGUE LIVES, USING MINER'S RULE WITH BOX BEAMS 2 THROUGH 8

Box Beam	Material	Environment	First Failure Blocks	Predicted* Failure Blocks	Notch** Condition
2	HY-80	Saltwater	7,080	8,031	K_t=3.26
3	HY-80	Saltwater	4,170	8,031	K_t=3.26
4	HY-80	Air	6,260	219,600	K_t=3.26
5	HY-130	Saltwater	996	472	K_t=3.13
6	HY-130	Air	2,146	59,873	K_t=3.13
7	17-4PH	Saltwater	3,051	3,897	K_t=3.00
8	17-4PH	Saltwater	1,226	1,120	K_t=3.00

*Based on $\Sigma n/N=1.0$ for condition specified.

**Stress concentration factors are assumed representative of as-welded conditions.

TABLE 7 — NOTCH CONDITIONS NECESSARY TO PREDICT BOX-BEAM FAILURES

Box Beam	Material	Environment	First Failure	Notch Condition
2	HY-80	Saltwater	7,080	3.7
3	HY-80	Saltwater	4,170	6.7
4	HY-80	Air	6,260	>20
5	HY-130	Saltwater	996	2.4
6	HY-130	Air	2,146	7.7
7	17-4PH	Saltwater	3,051	3.4
8	17-4PH	Saltwater	1,226	3.0

TABLE 8 — RESIDUAL TENSILE STRESS NECESSARY TO CAUSE BOX-BEAM FAILURES*

Box Beam	Material	Environment	First Failure	Residual Stress ksi
2	HY-80	Saltwater	7,080	10
3	HY-80	Saltwater	4,170	20
4	HY-80	Air	6,260	33
5	HY-130	Saltwater	996	None
6	HY-130	Air	2,146	30
7	17-4PH	Saltwater	3,051	6
8	17-4PH	Saltwater	1,226	None

*Stress-concentration factors are assumed representative of as-welded condition—K_t=3.00-3.26.

TABLE 9 — CLOSEST PREDICTIONS OF SURFACE-FLAW ANALYSES

Box Beam	Material	Environment	First Failure Blocks	Predicted Failure Blocks	Flaw Model
2	HY-80	Saltwater	7,080	5,998	UT-F-UR
3	HY-80	Saltwater	4,170	5,998	UT-F-UR
4	HY-80	Air	6,260	11,962	UT-F-UR
5	HY-130	Saltwater	996	1,097	EC-P-R
6	HY-130	Air	2,146	2,188	EC-P-UR
7	17-4PH	Saltwater	3,051	3,311	X-F-R
8	17-4PH	Saltwater	1,226	1,200	EC-P-R

Note: EC = eddy current; UT = ultrasonics; X = X-ray; F = Forman; P = Paris; R = retarded; UR = unretarded.

TABLE 10 — NOTCH GEOMETRIES

Nondestructive Testing Method	Initial Flaw Condition a_i in.	Initial Flaw Condition $2C_i$ in.	Root Radius ρ in.	a/ρ
Eddy Current	0.015	0.250	0.510	0.0294
Ultrasonics	0.060	0.188	0.102	0.03191
X-Ray	0.050	0.100	0.050	1.0

TABLE 11 — COMPARISON OF EQUATIONS FOR COMPUTING K_t

Nondestructive Testing Method	Equation (9) $1+2\sqrt{a/\rho}$	Equation (10) $0.78+2.24\sqrt{a/\rho}$	Equation (11)* Assumed K_f				
			2	2.5	3	4	5
Eddy Current	1.34	DNA**	DNA***				
Ultrasonics	2.5	DNA**	2.2	2.8	3.4	4.6	5.8
X-Ray	3.0	3.02	2.4	3.0	3.7	5.0	6.4

Notes:

DNA = Does not apply.

*Equation (11): $K_t = 1 + \frac{(K_f - 1)}{q}$

$q = 0.830$ for ultrasonics flaw

$q = 0.739$ for X-ray flaw.

**DNA - a/ρ not within limits $1 < a/\rho < 360$.

***DNA - ρ not less than or equal to 0.10.

TABLE 12 — TOTAL PREDICTED LIFE FOR BOX BEAMS 2 THROUGH 8

Box Beam	Life	Predicted Flaw-Growth Life	Flaw Model	Predicted Flaw Initiation	Total Life
2	7,080	5,998	UT-F-UR	206	6,204
3	4,170	5,998	UT-F-UR	206	6,204
4	6,260	11,962	UT-F-UR	245	12,207
5	996	921*	X-P-R	72	993
6	2,146	1,713	X-F-R	168	1,881
7	3,051*	3,057*	UT-P-R	154	3,211
8	1,226	1,200	EC-P-R	77	1,277

*Average Data Used.

Note: EC = eddy current; UT = ultrasonics; X = X-ray; F = Forman; P = Paris; R = retarded; UR = unretarded.

TABLE 13 — CRACK INITIATION AS PERCENTAGE OF TEST LIFE AND TOTAL PREDICTED LIFE

Box Beam	Predicted Life				Initiation as Percentage of Test Life	Initiation as Percentage of Test Predicted Life
	Test Life	Flaw Growth	Initi-ation	Total		
2	7,080	5,998	206	6,204	2.9	3.3
3	4,170	5,998	206	6,204	4.9	3.3
4	6,260	11,962	245	12,207	3.9	2.0
5	996	921	72	993	7.2	7.3
6	2,146	1,713	168	1,881	7.8	8.9
7	3,051	3,057	154	3,211	5.1	4.8
8	1,226	1,200	77	1,277	6.3	6.0
Average					5.4	5.1

TABLE 14 — CUMULATIVE DAMAGE CALCULATIONS FOR BOX BEAMS 2 AND 3

Stress Range (ksi)	n	N HY-80 Retemp. K_t=3.26	n/N	N HY-80 Retemp. Smooth Weld	n/N	N HY-80 As Rec'd Smooth	n/N
11.98	544	1.28×10^7	0.0000425	2.1×10^7	0.00002591	$> 10^8$	
15.20	312	7.4×10^6	0.00004216	1.25×10^7	0.00002496	8×10^7	0.0000039
18.86	138	4.2×10^6	0.00003286	7.4×10^6	0.000018649	4×10^7	0.00000345
46.36	1	5×10^5	0.0000020	5.0×10^5	0.000002000	2.8×10^6	0.000000357
40.72	3	7×10^5	0.000004286	5.8×10^5	0.000005172	4×10^6	0.00000075
29.57	1	1.4×10^6	0.000000714	2.8×10^6	0.000000357	9.8×10^6	0.000000102
Σ			0.000124519		0.000077043		0.000008559
Spectra to Failure			8,031		12,980		116,000+

Note: See Figure 14 for S-N curves.

TABLE 15 — CUMULATIVE DAMAGE CALCULATIONS FOR BOX BEAM 4

Stress Range (ksi)	n	N HY-80 K_t=3.26	n/N	N HY-80 Retemp. V-Notch	n/N	N HY-80 Retemp. Smooth	n/N
11.98	544	$>10^8$		$>10^8$		$>10^8$	
15.20	312	$>10^8$		$>10^8$		$>10^8$	
18.86	138	$>10^8$		$>10^8$		$>10^8$	
46.36	1	6.4×10^5	0.000001563	$>10^8$		$>10^8$	
40.72	3	1.1×10^6	0.000002727	$>10^8$		$>10^8$	
29.57	1	3.8×10^6	0.000000263	$>10^8$		$>10^8$	
Σ			0.000004553				
Spectra to Failure			219,600		Runout		Runout

Note: See Figure 17 for S-N curves.

TABLE 16 — CUMULATIVE DAMAGE CALCULATIONS FOR BOX BEAM 5

Stress Range (ksi)	n	N HY-130 Boeing K_t-3.13	n/N
19.50	544	1.05×10^6	0.000518
25.00	312	4.6×10^5	0.000678
31.34	138	2.2×10^5	0.000627
72.96	1	1.3×10^4	0.0000769
65.56	3	1.5×10^4	0.000200
47.31	1	5.8×10^4	0.0000172
Σ			0.002117793
Spectra to Failure			472
Note: See Figure 20 for S-N Curves.			

TABLE 17 — CUMULATIVE DAMAGE CALCULATIONS FOR BOX BEAM 6

Stress Range (ksi)	n	N HY-130 Boeing K_t-3.13	n/N
17.44	544	$>10^8$	
22.10	312	$>10^8$	
27.40	138	$>10^8$	
67.76	1	1.1×10^5	9.091×10^{-6}
59.38	3	4×10^5	7.5×10^{-6}
43.16	1	9×10^6	1.11×10^{-7}
Σ			1.6702×10^{-5}
Spectra to Failure			59,873
Note: See Figure 22 for S-N Curves.			

TABLE 18 — CUMULATIVE DAMAGE CALCULATIONS FOR BOX BEAM 7

Stress Range (ksi)	n	N 17-4PH K_t=2 Fig. 26	n/N	N 17-4PH K_t=3 Fig. 27	n/N	N 17-4PH K_t=4 Fig. 28	n/N
13.62	544	6.0×10^7	9.067×10^{-6}	1×10^7	5.44×10^{-5}	5×10^6	1.088×10^{-4}
17.22	312	2.0×10^7	1.56×10^{-5}	7×10^6	4.4571×10^{-5}	1×10^6	3.12×10^{-4}
21.26	138	9.0×10^6	1.533×10^{-5}	3×10^6	4.6×10^{-5}	8.5×10^5	1.6235×10^{-4}
53.58	1	1.5×10^5	6.667×10^{-6}	3×10^4	3.333×10^{-5}	3.8×10^4	2.6316×10^{-5}
45.68	3	4.0×10^5	7.5×10^{-6}	4×10^4	7.5×10^{-5}	7×10^4	4.2857×10^{-5}
33.90	1	8.5×10^5	1.176×10^{-6}	3×10^5	3.3333×10^{-6}	2×10^5	5.0×10^{-6}
Σ			5.5343×10^{-5}		2.56638×10^{-4}		6.57326×10^{-4}
Spectra to Failure			18,069		3,897		1,521

Note: See Figures 26-28 for S-N Curves.

TABLE 19 — CUMULATIVE DAMAGE CALCULATIONS FOR BOX BEAM 8

Stress Range (ksi)	n	N 17-4PH K_t=2 Fig. 26	n/N	N 17-4PH K_t=3 Fig. 27	n/N
18.48	544	1.5×10^{7}	3.6267×10^{-5}	5.0×10^{6}	1.088×10^{-4}
23.48	312	8.0×10^{6}	3.9×10^{-5}	1.0×10^{6}	3.12×10^{-4}
29.12	138	2.0×10^{6}	6.9×10^{-5}	7.0×10^{5}	1.97143×10^{-4}
71.50	1	2.0×10^{4}	5×10^{-5}	1.0×10^{4}	1.0×10^{-4}
63.32	3	5.5×10^{4}	5.4545×10^{-5}	2.0×10^{4}	1.5×10^{-4}
45.64	1	4.0×10^{5}	2.5×10^{-6}	4.0×10^{4}	2.5×10^{-5}
Σ			2.51312×10^{-4}		8.92943×10^{-4}
Spectra to Failure			3,979		1,120

Note: See Figures 26 and 27 for S-N Curves.

TABLE 20 — PREDICTED-LIFE VALUES FOR SURFACE FLAWS
(Predicted Life (Blocks))

Flaw-Model	Box Beam					
	2,3	4	5	6	7	8
EC-P-R	*	*	1,097	3,508	6,843	1,200
EC-P-UR	*	*	659	2,188	4,457	739
EC-F-R	*	*	578	1,564	2,351	445
EC-F-UR	10,792	*	344	1,077	1,729	284
UT-P-R	*	*	204	531	2,064	185
UT-P-UR	11,826	*	125	354	1,198	119
UT-F-R	*	*	134	300	716	84
UT-F-UR	5,998	11,962	41	97	381	27
X-P-R	*	*	854	3,894	9,761	1,057
X-P-UR	*	*	517	2,465	6,252	665
X-F-R	*	*	453	1,713	3,311	391
X-F-UR	14,755	*	241	1,129	2,500	240
Actual Failure	7,080 and 4,170	6,260	996	2,146	3,051	1,226

Note: EC = eddy-current flaw, 0.015 × 0.25 in.; UT = ultrasonic flaw, 0.06 × 0.188 in.; X = X-ray flaw, 0.05 × 0.10 in.; F = Forman; P = Paris; R = retarded; UR = unretarded.

*Predicted life >15,000 blocks.

TABLE 21 — SURFACE-FLAW ANALYSES — CLOSENESS OF PREDICTION

Rank	Box Beam Number — Model and Ratio of Predicted-To-Actual Life											
	2	(3)	4		5		6		7		8	
1	UT-F-UR	0.85 (1.44)	UT-F-UR	1.91	EC-P-R	1.10	EC-P-UR	1.02	X-F-R	1.09	EC-P-R	0.98
2	EC-F-UR	1.52 (2.59)		*	X-P-R	0.86	X-P-UR	1.15	X-F-UR	0.82	X-P-R	0.86
3	UT-P-UR	1.67 (2.84)			EC-P-UR	0.66	X-F-R	0.80	EC-F-R	0.77	EC-P-UR	0.60
4	X-F-UR	2.08 (3.54)			EC-F-R	0.58	EC-F-R	0.73	UT-P-R	0.68	X-P-UR	0.54
5	**				X-P-YR	0.52	X-F-UR	0.53	EC-F-UR	0.57	EC-F-R	0.36
6					X-F-R	0.45	EC-F-UR	0.47	EC-P-UR	1.46	X-F-R	0.32
7					EC-F-UR	0.35	EC-P-R	1.63	UT-P-UR	0.39	EC-F-UR	0.23
8					X-F-UR	0.24	UT-P-R	0.25	UT-F-R	0.23	X-F-UR	0.20
9					UT-P-R	0.20	X-P-R	1.81	UT-F-UR	0.12	UF-P-R	0.15
10					UT-P-UR	0.13	UT-P-UR	0.16	X-P-UR	2.05	UT-P-UR	0.10
11					UT-F-R	0.13	UT-F-R	0.14	EC-P-R	2.24	UT-F-R	0.07
12	**			*	UT-F-UR	0.04	UT-F-UR	0.05	X-P-R	3.20	UT-F-UR	0.02

Note: UT = ultrasonics; EC = eddy current; X = X-ray; F = Forman; P = Paris; R = retarded; UR = unretarded.

* all others > 2.40.

** all others > 2.12 (3.60).

TABLE 22 — REANALYSES OF SURFACE FLAWS, USING CRACK-GROWTH DATA

Surface	Box Beam Number	Model	Actual Life blocks	Predicted Life, Upper-Bound Data blocks	New Predicted Life blocks	Data Used
Eddy Current	5	Paris - retarded	996	1,097	1,298 1,188	Lower bound Average
Ultrasonics	5	Paris - retarded	996	204	238 220	Lower bound Average data
X-Ray	5	Paris - retarded	996	854	1,003 921	Lower bound Average
Ultrasonics	6	Paris - retarded	2,146	531	1,060 706	Lower bound Average data
Ultrasonics	7	Paris - unretarded	3,051	1,198	1,788	Average data
Ultrasonics	7	Paris - retarded	3,051	2,064	3,057	Average data

REFERENCES

Acronyms used in this list are defined as follows:

AIAA	American Institute of Aeronautics and Astronautics
SNAME	Society of Naval Architects and Marine Engineers
NSRDC	Naval Ship Research and Development Center
DTNSRDC	David W. Taylor Naval Ship Research and Development Center
VDI-Z	Verein Deutscher Ingenieure-Zeitschrift
NRL	Naval Research Laboratory

1. Beach, J.E. et al., "A Large-Scale Fatigue Evaluation of Hydrofoil-Foil Structures," SNAME/AIAA Advanced Marine Vehicles Conference (17-19 Apr 1978).

2. Palmgren, A., "Die Lebanstauer Von Kugellagern," VDI-Z, Vol. 68 (1924).

3. Miner, M.A., "Cumulative Damage in Fatigue," Journal of Applied Mechanics, Vol. 12 (1945).

4. Richards, C.W., Chapter 9, Engineering Materials Science, Wadsworth Publishing Company, San Francisco (1967).

5. Bixler, W.D. and D.D. Miller, "Slow Crack Growth, Fracture, Fatigue and Corrosion Assessment of Production PHM Struts and Foils," Boeing Document D312-80437-1 (1975).

6. "Structural Steel Design," Edited by L. Tall, Ronald Press Company, New York (1974).

7. "Welding Handbook, Section 1," Edited by A.L. Phillips, American Welding Society, p. 5.29 (1969).

8. Engle, R.M., "CRACKS II User's Manual," Structures Department, Air Force Flight Dynamics Laboratory, Dayton, Ohio, AFFDL-TM-74-173 (1974).

9. Marchica, N.V. et al., "A Fatigue-Crack Propagation Analysis Program Using Interactive Computer Graphics," Symposium on Applications of Computer Methods in Engineering (23-26 Aug 1977).

10. Clark, W.G. and S.J. Hudak, Jr., "Variability in Fatigue Crack Growth Rate Testing," Journal of Testing and Evaluation, Vol. 3 (Nov 1975).

11. Gross, M.R. and E.J. Czyryca, "Effects of Notches and Salt Water Corrosion on the Flexural Fatigue Properties of Steels for Hydrospace Vehicles," Naval Engineers Journal (Dec 1967).

12. Gross, M.R. and H.C. Ellinghausen, "Investigation of the Fatigue Properties of Submarine Hull Steels," U.S. Naval Engineering Experiment Station, R&D Report 910 178, S-R007-01-01 (31 Aug 1960).

13. Hydronautics, Incorporated, R.R. Moore Fatigue Data for HY-130 Steel, Test Frequency = 100,000 CPM," (1965).

14. Miller, D.D., "Hydrofoil Material Evaluation - Base Metal (& Coated Metal) Fatigue and Fracture Studies," Boeing Document D180-15197-3, (Nov 1974).

15. Barsom, J.M. et al., "Fatigue-Crack Propagation in High Yield-Strength Steels," Engineering Fracture Mechanics, Vol. 2, pp. 301-317 (1971).

16. Barsom, J.M. et al., "Corrosion-Fatigue Crack Propagation Below K_{ISCC} in Four High-Yield-Strength Steels," United States Steel, Project 89.021-024(3) (14 Dec 1970).

17. Crooker, T.W., "Effect of Heat Treatment on Corrosion-Fatigue Crack Growth," Enclosure to NRL letter 6384-9N (1974).

18. Crooker, T.W., et al., "Influence of Experimental Factors on Corrosion-Fatigue Crack-Growth Rate Characterization in 17-4PH Steel," Report of NRL Progress, pp. 21-23 (May 1976).

19. Crooker, T.W. et al., "Effects of Loading Parameters on Fatigue-Crack Growth in HY-130 Steel," NRL Memorandum Report 2822 (Jun 1974).

20. Crooker, T.W. and W.R. Cares, "An Exploratory Investigation of Corrosion-Fatigue Crack Growth in HY-130 Base Plate," NRL Memorandum Report 2660 (Oct 1973).

BIBLIOGRAPHY

Snow, R.S., "Fatigue Properties of Ship Steels and Weldments Determined by Cantilever-Loaded Rotating Beam Tests," Electric Boat Division, General Dynamics Corporation, Project M-898 (12 Jul 1961). (See Appendix A.)

INITIAL DISTRIBUTION

Copies		Copies	
1	DDR & E (Lib)	1	NASA Langley/Struc Div
1	DNL	1	MARAD/Office of R&D
1	CHONR 439	12	DDC
1	CNO (OP-098T)	1	LC/Sci & Tech Div
2	NAVMAT 1 MAT 033B 1 MAT 034B	1	DOT (R&T)
4	NRL 1 Code 6382 1 Code 6384 1 Code 8433 1 Tech Lib	1	NRC (Nat Acad Sci/Ship Hull Research Comm)
1	USNA/Lib	1	NSF (Engr Div)
1	NADC/30P72	2	Lehigh University 1 Dept of Mech 1 Dept of Civil Engr
7	NAVSEA 1 SEA 0322 1 SEA 035 2 SEA 03511 1 SEA 03522 1 PMS 303 1 PMS 304	1	MIT (Dept of Ocean Engr)
2	NAVAIR 1 Struc Br/5302 1 Engr Div/520	1	University of Virginia Civil Engr Dept
6	NAVSEC 1 SEC 6101D 1 SEC 6114D 1 SEC 6120D 2 SEC 6128 1 SEC 6129	1	SNAME
1	Wright-Patterson AFB/ AFFDL Struc Div/FBT	1	Aerojet General (Sur Eff Ships Div)
2	USCG 1 Chief Testing & Dev Div 1 Ship Structures Comm	1	Alcoa Research Labs
		1	American Bur of Shipping
		1	Bell Aerospace/New Orleans Opr
		1	Boeing Aerospace/Marine Div
		1	Grumann Aerospace/Marine Sys Prog. Manager
		3	Hayes, Seay, Mattern & Mattern/Mr. Ichter
		1	U.S. Steel Research Labs

CENTER DISTRIBUTION

Copies	Code
1	17
1	1702
2	1709
1	172
1	172.4
1	173
2	173.1
15	173.2
1	173.3
1	173.4
1	173.5
1	174
1	1770
1	178
2	2803
1	281
1	2814
1	282
1	2821
1	2822
1	2823
30	5214.1
1	522.1
1	522.2

DTNSRDC ISSUES THREE TYPES OF REPORTS

(1) DTNSRDC REPORTS, A FORMAL SERIES PUBLISHING INFORMATION OF PERMANENT TECHNICAL VALUE, DESIGNATED BY A SERIAL REPORT NUMBER.

(2) DEPARTMENTAL REPORTS, A SEMIFORMAL SERIES, RECORDING INFORMATION OF A PRELIMINARY OR TEMPORARY NATURE, OR OF LIMITED INTEREST OR SIGNIFICANCE, CARRYING A DEPARTMENTAL ALPHANUMERIC IDENTIFICATION.

(3) TECHNICAL MEMORANDA, AN INFORMAL SERIES, USUALLY INTERNAL WORKING PAPERS OR DIRECT REPORTS TO SPONSORS, NUMBERED AS TM SERIES REPORTS; NOT FOR GENERAL DISTRIBUTION.